The Tibetan Plateau Space-based Tropospheric Aerosol Climatology: 2007–2020

Honglin Pan[1,2,3,4,5,6], Jianping Huang[1]*, Jiming Li[1], Zhongwei Huang[1], Minzhong Wang[2,3,4,5,6], Ali Mamtimin[2,3,4,5,6], Wen Huo[2,3,4,5,6], Fan Yang[2,3,4,5,6], Tian Zhou[1], Kanike Raghavendra Kumar[7]

[1]*Collaborative Innovation Center for Western Ecological Safety, College of Atmospheric Sciences, Lanzhou University, Lanzhou, 730000, China*

[2]*Institute of Desert Meteorology, China Meteorological Administration, Urumqi, 830002, China*

[3]*National Observation and Research Station of Desert Meteorology, Taklimakan Desert of Xinjiang, Urumqi, 830002, China*

[4]*Taklimakan Desert Meteorology Field Experiment Station of China Meteorological Administration, Urumqi, 830002, China*

[5]*Xinjiang Key Laboratory of Desert Meteorology and Sandstorm, Urumqi, 830002, China*

[6]*Key Laboratory of Tree-ring Physical and Chemical Research, China Meteorological Administration, Urumqi, 830002, China*

[7]*Department of Engineering Physics, College of Engineering, Koneru Lakshmaiah Education Foundation, Vaddeswaram, Guntur 522302, Andhra Pradesh, India*

Correspondence: Jianping Huang (hjp@lzu.edu.cn)

Abstract. A comprehensive and robust dataset of tropospheric aerosol properties is important for understanding the effects of aerosol-radiation feedback on the climate system and reducing the uncertainties of climate models. The third pole of Earth (Tibetan Plateau, TP) is highly challenging to obtain long-term in situ aerosol data due to its harsh environmental conditions. Here, we provide the more reliable new vertical aerosol index (AI) parameter from the spaceborne-based Lidar CALIOP onboard CALIPSO for daytime and nighttime to investigate the aerosol's climatology over the TP region during 2007-2020. The calculated vertical AI was derived from the aerosol extinction coefficient (EC), which was rigorously quality-checked and validation, and validated for passive satellite sensors (MODIS) and ground-based LIDAR measurements. Generally, our results demonstrated that there was agreement of the AI dataset with the CALIOP and ground-based LIDAR. Besides, the results showed that after removing the low-reliability aerosol target signal, the optimized data can obtain the aerosol characteristics with higher reliability. The data also reveals the patterns and concentrations of high-altitude vertical structure characteristics of the tropospheric aerosol over the TP. It will also help to update and make up the observational aerosol data in the TP. We encourage climate modelling groups to consider new analyses of the AI vertical patterns, comparing the more accurate datasets, with the potential to increase our understanding of the aerosol-cloud interaction (ACI) and aerosol-radiation interaction (ARI) and its climate effects. Data described in this work are available at https://data.tpdc.ac.cn/en/disallow/03fa38bc-25bd-46c5-b8ce-11b457f7d7fd

DOI:10.11888/Atmos.tpdc.300614. (Honglin Pan et al., 2023).

Keywords: Tibetan Plateau, CALIPSO, Aerosol index vertical structure, Tropospheric aerosols, Aerosol climatology.

1 Introduction

The three poles (i.e., the Arctic, the Antarctic and the Tibetan Plateau (TP)) have the highest mountains in the world and store more snow, ice and freshwater than any other place. The unique geographical location of the Antarctic, the Arctic, and the TP has unique ecological, climatic, and natural environmental changes. Also, the three locations have a crucial role in global and regional climate change. However, studies have found that these regions are susceptible to climate change. The differences in these regions may also affect key feedback loops for global climate change and the sustainability of human life. Unfortunately, our understanding of the three poles, particularly the relations between the regions, remains limited due to insufficient observation data. Currently, the collection of additional research data for these extreme environments is one of the major bottlenecks in facilitating comprehensive studies of these regions. Sufficient attention has been given to the polar regions and the TP in successive IPCC reports (IPCC, 2013 and 2021). The similarities between TP and the other two polar regions are their low temperatures, remote location, and large water storage capacity. On the other hand, TP has a more highly complex climate than the Arctic and the Antarctic (where ice is the primary medium) and its land surface (including forests, grasslands, bare soil, lakes and glaciers) is more diverse. These differences make the transport and accumulation of pollutants in the TP region different from the other two polar regions.

TP is known as the "Third Pole" because it has the third largest ice mass on Earth, after the Antarctic and the Arctic regions (Qiu, 2008). TP also called the "Asia Water Towers", provides fresh water to 40% of the world's population due to its vast water reserves such as glaciers, lakes and rivers (Immerzeel et al., 2010). Furthermore, TP is the "Roof of the World", which covers an area of ~2.5 million km^2 at an average altitude of about 4,000 m a.s.l. (above sea level) and includes all of Tibet and parts of Qinghai, Gansu, Yunnan, and Sichuan in southwestern China, as well as parts of India, Nepal, Bhutan, and Pakistan (Nieberding et al., 2020). To the north of the TP region is situated by the Taklamakan Desert (TD) (see Figure 1). This high altitude and specific

topographic area effectively serve as a heat source during the spring (MAM) and summer (JJA) months. This thermal structure helps the TP to function virtually as an "air pump", attracting warm and humid air from the lower latitude oceans by suction (Yanai et al., 1992; Wu and Zhang, 1998; Wu et al., 2007; Wu et al., 2012). Consequently, large-scale mountains play a crucial role in shaping regional and even global weather and climate through mechanical and thermodynamic effects and affect the global energy-water cycle (Xu et al., 2008; Molnar et al., 2010; Boos and Kuang, 2010; Wu et al., 2015). It is closely related to the survival of human beings in the world.

Climate projections are simulated responses of the climate system to future emission or concentration scenarios of greenhouse gases (GHGs) and aerosols and are generally calculated using climate models. The reasons for the gap between models and observations may also be due to inadequate solar, volcanic, and aerosol forcing used in the models, and in some modelling, may be due to an overestimation of the response to increasing GHG and other anthropogenic forcing (the latter includes the role of aerosols). The most significant uncertainties in predicting future climate change are related to uncertainties in the distribution and properties of aerosols and clouds, their interactions, and limitations in the representation of aerosols and clouds in global climate models (IPCC, 2021). The primary aerosol types over the TP is dust, which is primarily contributed from the Taklimakan Desert (Liu et al.,2008; Chen et al., 2013;2022; Xu et al., 2015). Previously some studies of aerosol-cloud interaction (ACI) and aerosol-radiation interaction (ARI) have been conducted (Liu et al., 2022). For example, the dust aerosols lifting over the TP reduce the radius of ice particles in the convective clouds and prolong the cloud lifetime through the indirect radiation effect, which can lead to the development of higher convective clouds. The dust-affected convective clouds move further eastward under the action of westerly winds and merge with local convective cloud masses, triggering heavy precipitation in the Yangtze River Basin and northern China downstream of the TP (Z. Liu et al., 2019; Y. Liu et al., 2019). However, the effect of aerosol on the atmospheric energy and water cycle remains uncertain, mainly due to the lack of long-term and accurate vertical aerosol optical properties dataset over the TP region. This can help better understand aerosol's impact

on the atmospheric heating rate and stabilization and the subsequent cloud-precipitation process. Therefore, constructing a more long-term and reliable vertical dataset of aerosol optical parameters can make up the observational facts for aerosol-related study and provide a scientific basis for improving the global climate model simulation over the TP.

Generally, the primary aerosol optical parameters (such as extinction coefficient (EC), and aerosol optical depth (AOD)) acquisition method is in situ observations, which have high precision. However, in situ observations are restricted by the distribution of measurement stations over the TP. Hence, the resulting data lack spatial continuity, making it difficult to meet the objectives of growing regional atmospheric environmental studies (Chen et al.,2022; Goldberg et al.,2019; Giles et al., 2019). Satellite remote sensing (active and passive) is an effective tool for collecting aerosol optical information (including the vertical structure and spatial distribution) over a wide range of spatial scales, significantly offsetting the deficiencies of in situ observations. Satellite remote sensing can tackle difficulties connected to insufficient data and uneven geographical distributions to a certain extent (Chen et al., 2022; Wei et al.,2021). While for aerosol products observed from the Cloud-Aerosol Lidar and Infrared Pathfinder Satellite Observations (CALIPSO), the presence of some low-reliability aerosol target (LRAT) caused by cloud contamination, solar noise contamination, especially in the daytime, and ground clutter among mostly aerosol observations skews the distribution of the aerosol EC towards larger values, at least some of which may be identified as aerosols and retained in the analysis, makes the presence of some low confidence aerosol targets bias the distribution of aerosol extinction in most aerosol observations. The distribution of the aerosol EC will show greater biased values (Thomason and Vernier, 2013; Kovilakam et al., 2020; Pan et al., 2020; Kahn et al., 2010), and then will further enhance the aerosol index (AI) value due to the influence of radiation transfer interaction between clouds and the absorption layer, which will not truly reflect the differences in aerosol physical properties (Guan et al., 2008; Liu et al., 2019; Kim et al.,2018). Hence, gaining high confidence in EC helps us analyze aerosol optical properties and leads to numerous pertinent uses of EC data, which is essential for

148 accurately characterizing the upper range of aerosol ECs that occur on the TP.

149 The present study provides a dataset of monthly averaged vertical structure
150 characteristics of tropospheric high confidence aerosol optical properties including EC,
151 AOD, Angstrom exponent (AE), and aerosol index (AI) in the daytime and nighttime
152 over the TP and surrounding areas. The data for the above-mentioned optical properties
153 were retrieved based on the space-borne Lidar CALIOP (Cloud-Aerosol Lidar with
154 Orthogonal Polarization) on board the CALIPSO satellite for the period 2007-2020.
155 The main objective of this study is to calculate new and high-confidence aerosol optical
156 parameters of AI in the vertical distribution, by the strict quality control and validation
157 for passive remote sensing satellite sensor (MODIS) and active remote sensing ground-
158 based LIDAR. AI is dependent on aerosol concentration, optical properties and altitude
159 of the aerosol layer. Also, AI is particularly sensitive to high-altitude aerosols, which is
160 used to indicate small particles (those that act as cloud condensation nuclei) with a high
161 weight (Guan et al., 2010; Buchard et al., 2015; Liu et al., 2019; Nakajima et al., 2001).
162 The comprehensive data set of aerosol optical properties utilized in the study is of
163 substantial importance for understanding the impact of aerosol on the ecosystem and
164 reducing the uncertainties of climate models.

165 The data set used in this study is more effective to characterize the vertical
166 structure of aerosols while following standardized quality control methods to obtain
167 higher confidence in the aerosol vertical structural properties covariate data sets and
168 allow for comparison and application to the study of climate models and other
169 atmospheric science related problems between our records and other public different
170 data sets. To ensure meaningful confidence estimates, it is necessary to apply carefully
171 the following correction procedures and analytical validation for the constructed
172 aerosol covariates over the TP. The main steps to construct the dataset are grouped as
173 follows: (1) Removing the low-confidence aerosol EC at 532 nm and 1064 nm caused
174 by the misclassification of cloud and other interferences (e.g., surface clutter,
175 hygroscopicity etc.). Based on this, an interquartile range (IQR) method (see section
176 2.2) is utilized to discard the low confidence targets, and further obtain the monthly
177 averaged aerosol EC for day and nighttimes with higher confidence; (2) the pseudo-

Ångström exponent (hereafter AE) is calculated using the aerosol EC at 532 nm and 1064 nm with higher confidence; (3) obtaining vertical AI by the product of the AOD (the vertical layers integral of EC) and AE. (4) Validation for the constructed AI with MODIS and in situ LIDAR measurements using the standardized frequency distributions.

2 The construction of the data set

2.1 Study area

Figure 1 depicts the geopotential height of the TP and its surrounding areas (27-42°N,75-102°E, about 4,000 m a.s.l.), and a schematic diagram of CALIPSO satellite ground track over the TP in different months. The role of the "heat-driving air pump" of the TP provides abundant water vapor for the formation of clouds (Luo et al., 1984; Liou et al.,1986). Furthermore, the TP environment is greatly affected by natural and anthropogenic aerosols from the surrounding regions (Chen et al., 2013; Bucci et al.,2014; Xu et al.,2015). The strong convection generated by the TP will promote aerosols' vertical transport and increase aerosols' content in the troposphere and stratosphere (Vernier et al., 2015; Liu et al., 2022). Aerosols also serve as cloud condensation nuclei (CCN) or ice nuclei (IN), modifying cloud structure properties and precipitation (Twomey et al.,1977). Hence, the TP has been called as the pumping pump of water vapor, the cloud incubator, and the sand dust transfer station. By delivering water vapor, clouds, and dust, it regulates extreme weather and climate in the downstream and surrounding areas. It can be seen that the TP plays a crucial role in the impact and regulation of global and regional climate or environments (Luo et al.,1984; Rossow et al., 1999; Wan et al.,2017; Liu et al., 2022).

208
209
210
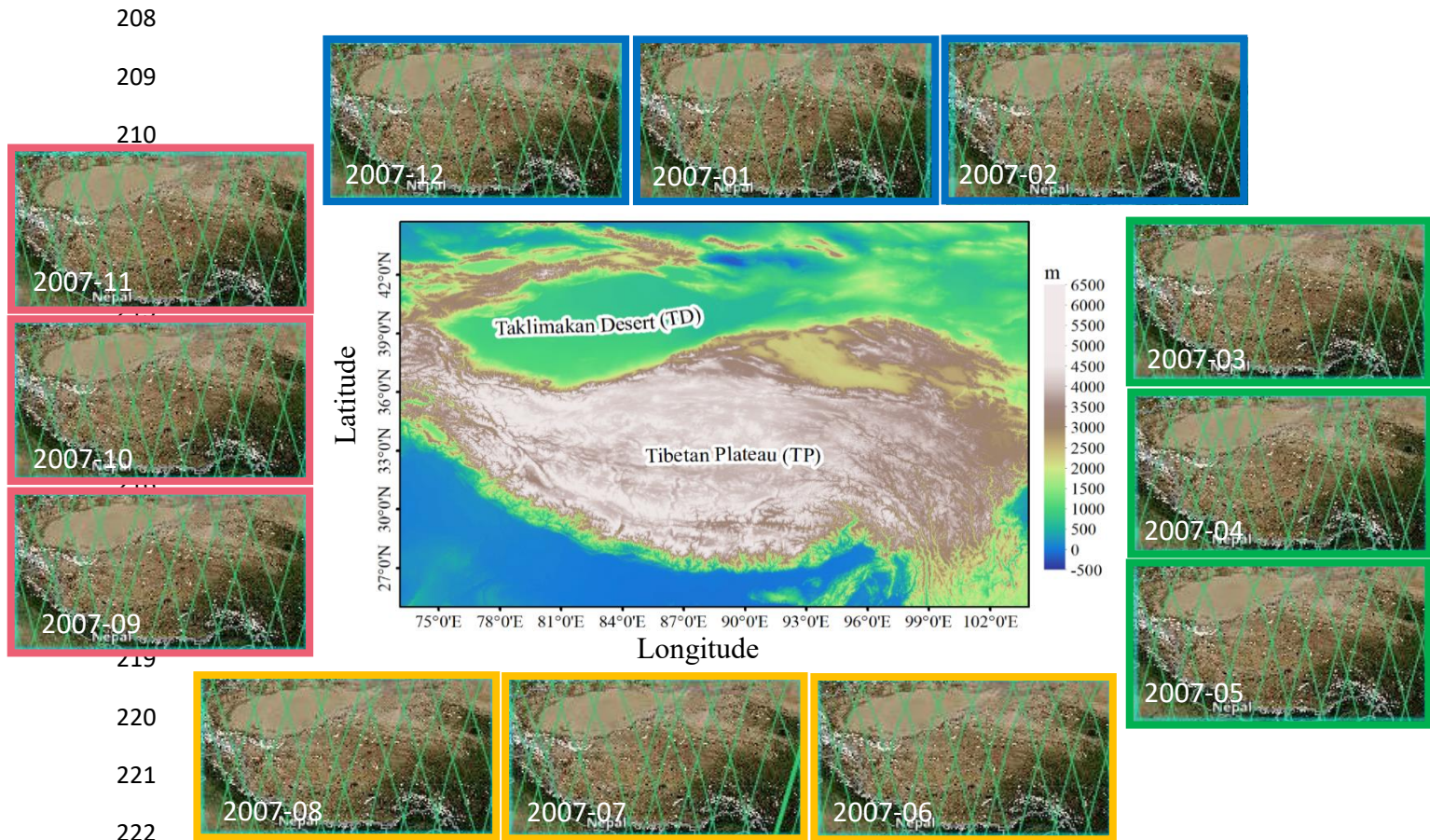
Figure. 1 The geopotential height of the TP and its surrounding areas (27-42°N,75-102°E). The schematic diagram of the transit of the CALIPSO satellite orbits over the TP in all months of 2007 (with 2007 as an example). The seasons have been classified as March-May is spring, June-August is summer, September-November is autumn, and December-February is winter).

2.2 CALIOP data and low-reliability aerosol target (LRAT) clearing method

The CALIOP, onboard the CALIPSO satellite was launched by the NASA on 28 April 2006, is the nadir-pointing dual-wavelength polarization Lidar, which can provide global and continuous information on the vertical distribution of aerosols and clouds at 532 nm and 1064 nm for daytime and nighttime (Winker e t al., 2007 and 2009). The CALIPSO-CALIOP (version 4.20) level-2 aerosol profile product is selected in this study, with vertical and horizontal resolutions of 60 m and 5 km, respectively. The used parameter includes Extinction_Coefficient_532 and Extinction_Coefficient_1064 between daytime and nighttime observations from 2007 to 2020. It should be noted that the CALIOP data uses as few instruments as necessary to complete the monthly aerosol climatology. We make this decision to limit the impact of differences between

238 instruments due to measurement techniques and wavelength range as well as assess the

239 general quality of the instrument's data set.

240   The presence of some low-reliability aerosol target (LRAT) caused by cloud

241 contamination, solar noise contamination, especially in the daytime, and ground clutter

242 among mostly aerosol observations skews the distribution of the aerosol EC toward

243 larger values (Thomason and Vernier, 2013). Consequently, to eliminate the LRAT, a

244 statistical approach to identify LRAT and extreme outliers is utilized based on the

245 interquartile range (IQR). IQR is a more conservative measure of the spread of

246 distribution than standard deviation (Iglewicz and Hoaglin, 1993). Note that this

247 technique is based on median statistics rather than the mean due to the skewed

248 distribution of EC. In our implementation, we used daily data at each altitude (0.06 km)

249 and latitude (0.05°) bin from 2007-2020 to determine frequency distribution of EC for

250 different months. Besides, we used the lower quartile (Q1) and upper quartile (Q3) of

251 the underlying distribution to find IQR, defined as Q3-Q1, a good measure of the spread

252 in the data relative to the median. Here, an extreme outlier is defined as Q3 + (3.5×IQR),

253 and a more upper outlier (Q3+(1.5×IQR)) is used for comparison (Iglewicz and Hoaglin,

254 1993). Meanwhile, the extreme outlier threshold is used to clear LRAT-affected

255 observations from the data set, which is better and more effective at identifying outliers

256 in the density distribution (Kovilakam et al., 2020).

257 **2.3 AI Data Processing**

258   According to the method described in section 2.2, the aerosol EC (observed at 532

259 nm and 1064 nm for daytime and nighttime) with higher reliability over the TP is

260 obtained. The monthly mean Ångström exponent (hereafter "pseudo-Ångström

261 exponent (AE)") for daytime and nighttime is derived to establish the 14-year aerosol

262 climatology (2007-2020) based on equation (1). The AE model for EC which is

263 wavelength dependence at 532 and 1064 nm is given by Kovilakam et al. (2020):

$$EC_{-532[m,i,j]} = EC_{-1064[m,i,j]} \left(\frac{\lambda_{532}}{\lambda_{1064}} \right)^{AE[m,i,j]}$$

264   (1)

265 where $EC_{\_532[m,i,j]}$ and $EC_{\_1064[m,i,j]}$ are extinction coefficients at 532 nm and 1064 nm,

266   respectively; AE [m, i, j] is the pseudo-Ångström exponent (Rieger et al.,2015;2019);

267   and the indices [m, i, j] represent the month, latitude, and altitude respectively.

268    $(\lambda_{532}/\lambda_{1064})$ represents the ratio of wavelengths at 532 nm and 1064 nm. The AE is

269   gridded to 0.05 ° latitude and 0.06 km altitude resolution. Further, the vertical

270   distribution of AI is calculated according to equation (2). AI has been developed by

271   Nakajima et al. (2001) and Liu et al. (2019) with the equation given below:

272    $$AI_{[m,i,j]} = AOD_{[m,i,j]} \times AE_{[m,i,j]} \tag{2}$$

273   Where $AI_{[m,i,j]}$ and $AOD_{[m,i,j]}$ are aerosol index and aerosol optical depth, respectively;

274    $AE_{[m, i, j]}$ is the pseudo-Ångström exponent; and [m, i, j] represent the month, latitude,

275   and altitude respectively. Note that to match the AE, AOD is also transformed into the

276   vertical distribution (not the column parameter). As we focus on the characteristics of

277   aerosols in the troposphere over the TP, we took samples from the surface at an altitude

278   of 12 km with a vertical resolution of 0.06 km. We integrated the EC of each two layers

279   to obtain an AOD, which corresponds to the average of the AE values of each two layers.

280   This achieves spatial matching between AOD and AE at the vertical heights. In the later

281   stage, when using the AI obtained from MODIS for comparative testing, we used the

282   PDF (probability density function) and average values of AI for characterization

283   displayed to facilitate comparison due to the differences in horizontal and vertical space.

284   The data in this manuscript are all based on the vertical structural distribution of

285   altitude-latitude with vertical and horizontal resolutions of 60 m and 0.05 ° ,

286   respectively. The monthly mean climatology of AI is retrieved from the CALIOP and

287   computed in altitude and latitude at 532 nm and 1064 nm for the daytime and nighttime

288   data sets.

289   **2.4 Aqua-MODIS satellite data**

290   Like the CALIPSO, Aqua is part of the A-Train constellation of satellites.

291   Therefore, the MODIS (Moderate-resolution Imaging Spectroradiometer) onboard

292   Aqua can achieve near-simultaneous observations of clouds and aerosols with

293   CALIPSO-CALIOP (less than two minutes) (Winker et al., 2007; Hu et al., 2010). The

294   Aqua satellite was successfully launched on May 4th, 2002. Aqua is the afternoon star,

passing through the equator from south to north at around 13:30 local time. The observation data of 36 wavebands were obtained, with a maximum spatial resolution of 250 m and a scanning width of 2330 km. MODIS is a passive imaging spectroradiometer, and there are a total of 490 detectors distributed in 36 spectral bands, with full spectral coverage ranging from 0.4 microns (visible light) to 14.4 microns (thermal infrared). In this study, Level 3 data (MYD08_M3) on a 1°×1° (longitude × latitude) gridded box is utilized. As shown in Table 1, MODIS can provide AOD and AE products at 550 nm wavelength. It is worth mentioning that we chose this data because MODIS data is widely used and has certain reliability in aerosol research. The parameters of AE and AOD from MODIS are also used to calculate the AI, which is applied to evaluate the monthly mean climatology of AI from CALIOP over TP (see Table 1).

Table 1 Comparison between MODIS and CALIOP existing data products (√ represents the existing data products of the satellite, NAN indicates non-existent, × represents non-existent data product parameters that need further calculation in this study).

Detector/Satellite	Wavelength	Extinction Coefficient (EC)	Aerosol Optical Depth (AOD)	Angstrom Exponent (AE)	Aerosol Index (AI)
CALIOP/CALIPSO (active)	532nm&1064nm	√	√	×	×
MODIS/Aqua (passive)	550nm	NAN	√	√	×

2.5 Ground-based LIDAR data

Besides, we used the ground-based LIDAR (Light Detection and Ranging) (38.967 ° N, 83.65 ° E, 1099.3m) detection data from the hinterland of the Taklimakan Desert (TD) to verify the validity and accuracy of the low confidence aerosol removal method and the AI calculated by CALIOP detection data. Multi-band Raman polarization LIDAR (hereafter LIDAR) is mainly used for the detection of dust, aerosols, and cloud particles in the atmosphere, which detection belongs to "Belt and

318 Road" Lidar Network from Lanzhou University, China (http://ciwes.lzu.edu.cn/), has

319 an advantage with calibrate or validate Satellite observation (see Figure 2). The primary

320 technical specifications of LIDAR are mentioned in Table 2. For the performance of

321 LIDAR and the data inversion of aerosol-related optical parameters, the authors advise

322 the readers to refer to the research work of Zhang et al. (2022, 2023).
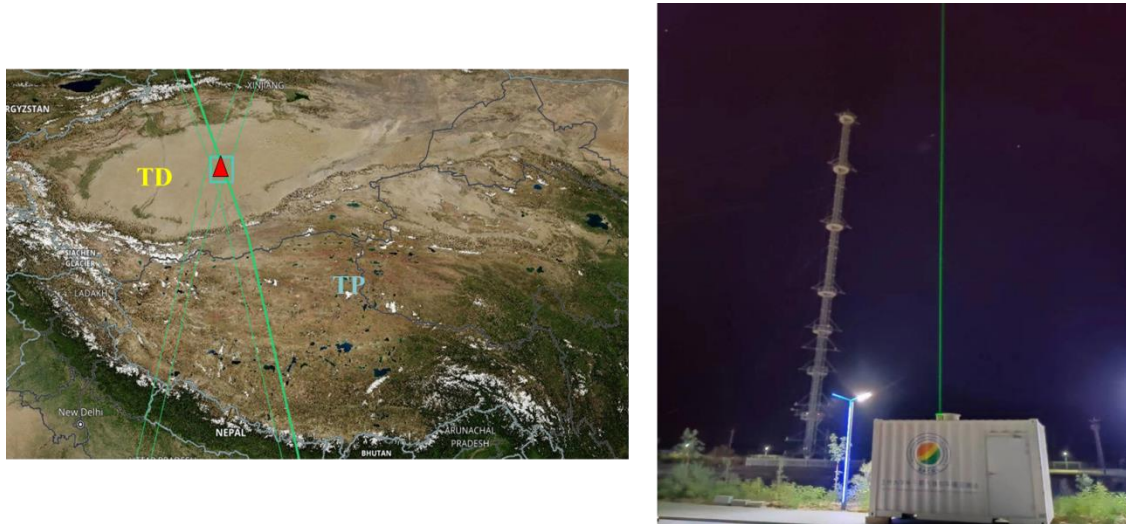
323

324 Figure 2. CALIPSO satellite orbit passes through the central area of the Taklimakan Desert

325 hinterland-left (the red triangle represents the observation coordinates of the ground-based LIDAR

326 - right (38.967 ° N, 83.65 ° E, 1099.3m), TD - Taklimakan Desert, TP - Qinghai Tibet Plateau)

327 (pictures from NASA'S Earth data (left) and photography(right)).

328 Table 2. Basic technical specifications of LIDAR from the hinterland of the Taklimakan Desert (TD).

Detection range	Spatial resolution	Laser wavelength	Laser energy	Pulse frequency
0~20km	7.5m	532nm/1064nm	100mJ	20Hz

329

330   In this study, based on the Level_2 aerosol profile data product (extinction

331 coefficient, EC) for daytime and nighttime detected by CALIOP from 2007 to 2020,

332 the low-reliability aerosol target (LRAT) is screened and eliminated. The aerosol

333 characteristic data set with higher reliability over the TP is constructed, and the data set

334 is verified and compared with MODIS and ground-based LIDAR to test its

335 effectiveness and accuracy. Thus, the vertical structure of aerosol properties and its

336 climatology with higher reliability over the TP can be obtained, providing adequate

337 observation facts and a basis for the TP. All steps were implemented and processed as

338 follows shown in Figure 3.
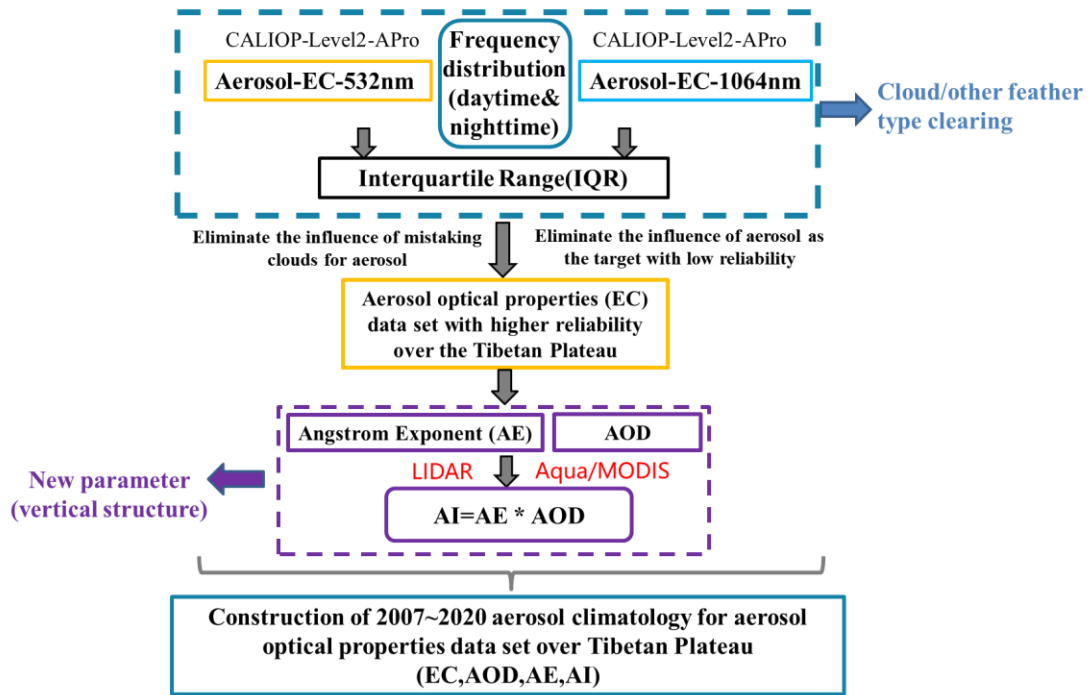
339

340 Figure 3. Flow chart of the construction and calculation process of aerosol optical characteristics

341 data set over the TP.

3 Results and discussion

3.1 Screening and elimination of Low-Reliability Aerosol Target (LRAT)

344   In this section, we screened and eliminated LRAT for tropospheric aerosol EC

345 from the CALIOP over the TP, based on the statistical method (see Section 2.2). Figures

346 4 and 5 show the monthly frequency distribution of EC detected by the CALIPSO-

347 CALIOP at 532 nm and 1064 nm in the daytime during 2007-2020. While Figures 6

348 and 7 are the same, but for the nighttime. It is observed that all Figures 4-7 demonstrated

349 the non-normal distribution of aerosol EC for the daytime and nighttime. It is found

350 that the upper outlier appeared to remove many enhanced aerosol measurements when

351 more sand and dust events occurred in the surrounding areas and rose to the TP in spring

352 and summer. In contrast, the extreme outlier was effectively identified in the frequency

353 distribution. Therefore, the extreme outlier threshold is used to clear LRAT

354 observations from the CALIOP data set which is necessary.

355   After the screening and elimination of LRAT, the monthly aerosol climatology

data and extreme outliers are compared for the years 2007-2020. We found that during the daytime for 532 nm and 1064 nm, the aerosol EC over the TP is mainly concentrated between 0 and 0.2. The extreme outliers in July and August are more significant than those in other months, related to the rising motion of the TP as a heat source in summer to trigger convection. This results in more ice clouds in the upper air, thus increasing the probability of misclassification of the cirrus anvil as an aerosol (Carrió et al., 2007; Kojima et al., 2004; Seifert et al., 2007). Also, the aerosol data points (samples) are the largest in May and the smallest in November over TP. Obviously, the aerosol samples are more in the spring and summer seasons than in autumn and winter. This is related to the frequent sand and dust activities in the spring and summer seasons around the TP (such as the Taklimakan Desert) and anthropogenic pollution (Y. Liu et al., 2019, as mentioned earlier).

Similarly, during the nighttime for 532 nm and 1064 nm, the aerosol EC over the TP is mainly concentrated between 0 and 0.1, and the extreme outliers in July and August are more significant than those in other months. However, the aerosol EC observed in the nighttime is smaller than the daytime data set. The primary consideration is that the daytime solar noise is considerable and the signal-to-noise ratio of LIDAR observation is low, which further increases the probability that the aerosol EC presents a skewed distribution; It can be seen that the elimination of LRAT from daytime data is more conducive to improving the accuracy of data. Meanwhile, the aerosol data points are the largest in April and the smallest in December over the TP. It can be seen that in April (spring), more aerosol samples were lifted and transported to the TP. Numerous observations have shown elevated dust plumes lofted into the free troposphere during spring, and air parcels between 4 km and 7 km mainly originate from the TD (Huang et al.,2008; Sasano,1996; Liu et al.,2008; Zhou et al.,2002; Matsuki et al., 2003). It is the same as the daytime with spring and summer being more than autumn and winter, while there is one order of magnitude larger than the daytime data. It is not difficult to see that the CALIOP is less sensitive during daytime than nighttime due to signal-noise-ratio reduction by solar background illumination, which leads to weakly scattering layers can be detected during nighttime while missed during

daytime (Huang et al., 2013; Liu et al.,2009).
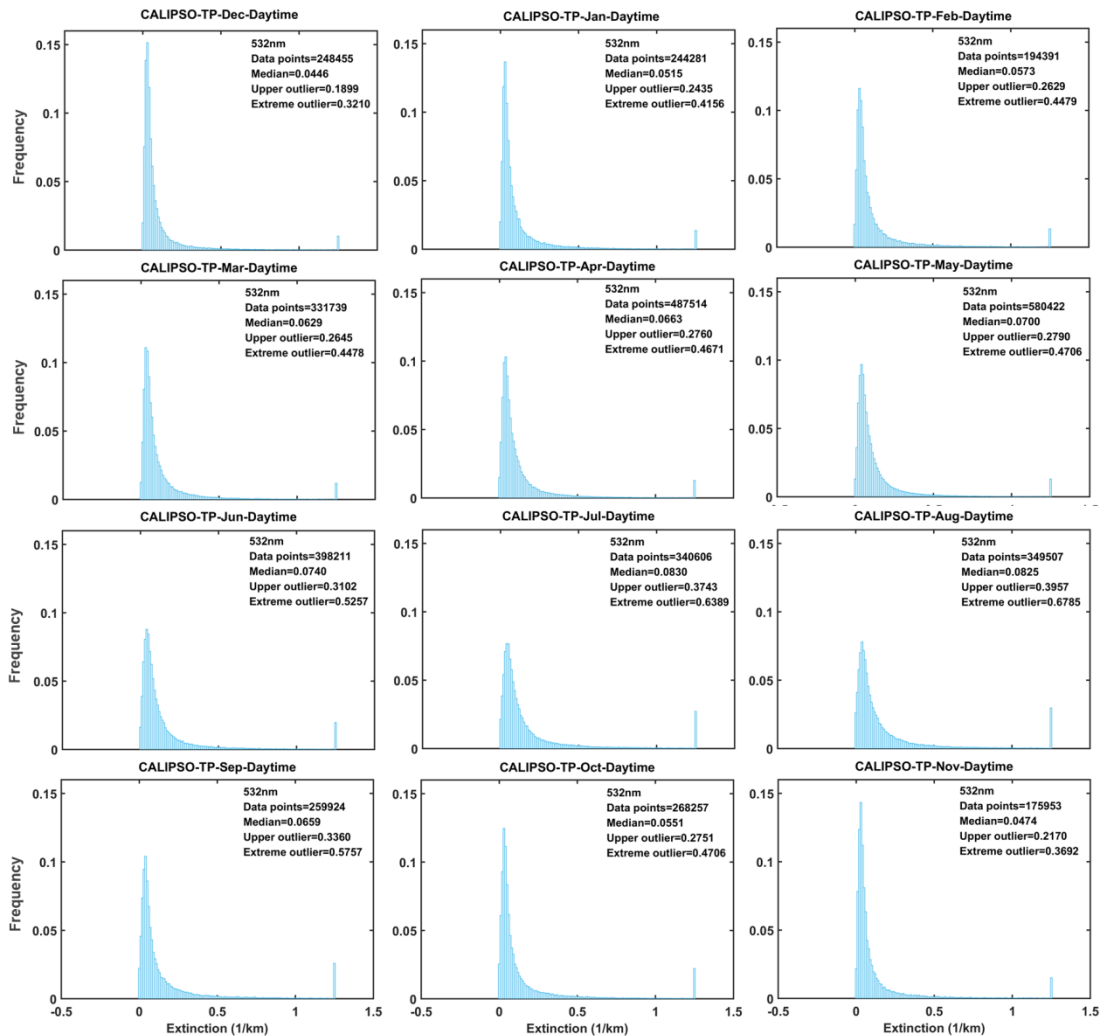
Figure 4. Monthly frequency distribution of aerosol extinction coefficient at 532 nm over the Tibet Plateau (TP) in the daytime during 2007-2020 from January to December (Panels in the first, second, third, and fourth rows corresponds to Winter (December-February), Spring (March-May), Summer (June-August), and Autumn (September-November). The frequency distribution is the number of events normalized to the maximum value. The Upper outlier, extreme outlier and median are also shown in all panels.
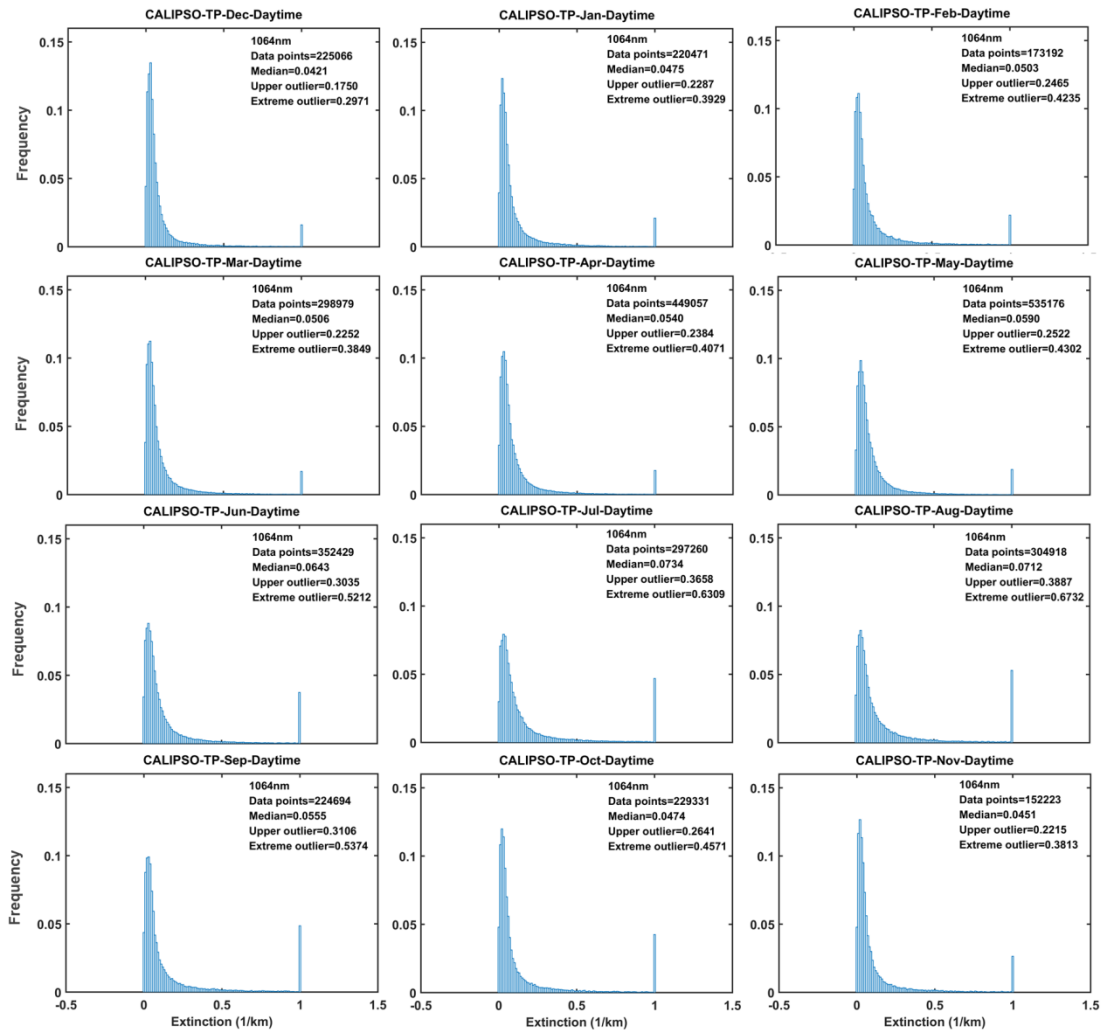
Figure 5. The same as in Figure 4, but for 1064nm.

398
399
400
401
402
403
404
405
406
407
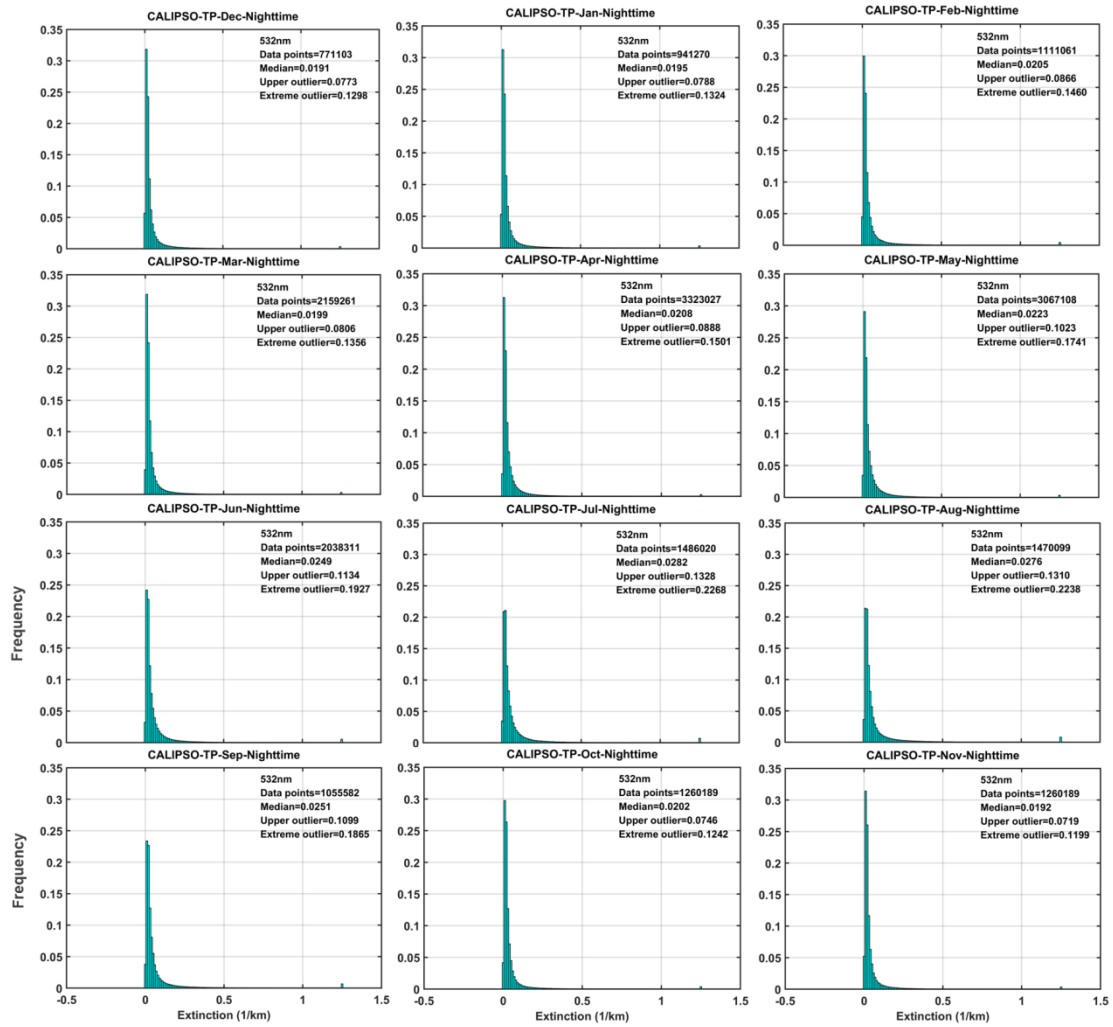
408

409 Figure 6. Monthly frequency distribution of aerosol extinction coefficient at 532 nm over the Tibet

410 Plateau (TP) in the nighttime during 2007-2020 from January to December (Panels in the first,

411 second, third, and fourth rows corresponds to Winter (December-February), Spring (March-May),

412 Summer (June-August), and Autumn (September-November). The frequency distribution is the

413 number of events normalized to the maximum value. The Upper outlier, extreme outlier and median

414 are also shown in all panels.

415
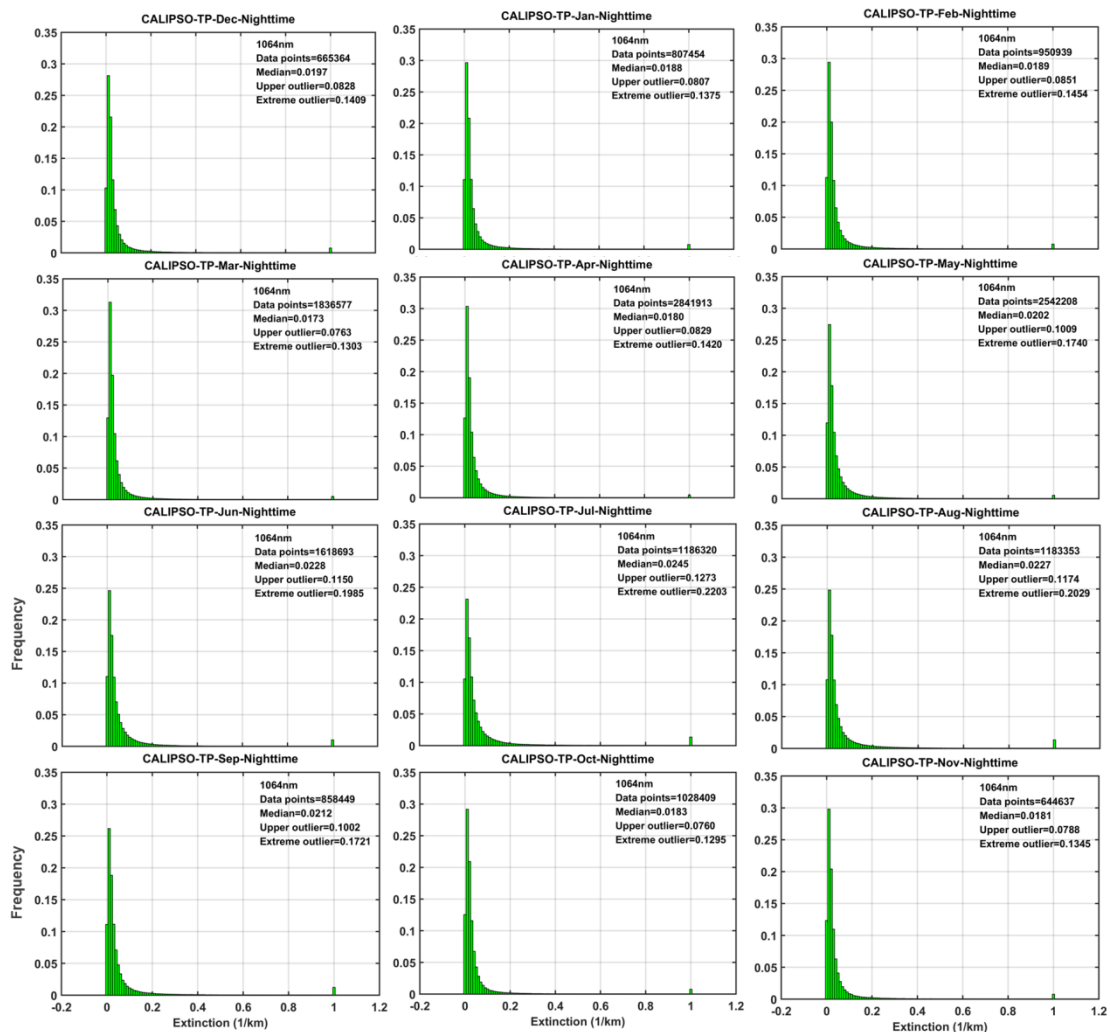
Figure 7. The same as in Figure 6, but for 1064 nm.

3.2 Constructing vertical aerosol index (AI) for daytime and nighttime

Figures 8 and 9 show daytime altitude-latitude plots of the monthly climatology of aerosol EC at 532 nm and 1064 nm before and after the screen, respectively. The monthly mean climatology of the pseudo-Ångström exponent (AE) and Aerosol Index (AI) vertical structure is then computed as shown in Figure 10. We choose typical months of January, April, July, and October to represent the respective seasons of winter, spring, summer, and autumn. Figures 8 and 9 show that extreme outliers in the troposphere over the TP have been eliminated, especially in the lower layer, where more obvious LRAT have been identified and eliminated. In the upper layer (more than 7 km), especially in April and July (i.e., spring and summer), weak cirrus signs may exist in the original aerosol signals and be eliminated. Compared with other seasons, the aerosol on the TP is widely and uniformly distributed in the troposphere in April, indicating

that in general, more aerosol loads are lifted over the TP in April. In Figure 10, we compute values between 0 and -1 for much of the troposphere and occasionally are between 0 and 2 in the middle troposphere (less than 8 km), which has similar results or pattern in Kovilakam's study (Kovilakam et al., 2020). Note that the derived value for pseudo-AE is without the physical meaning, and it is simply a means to combine AOD to obtain AI of vertical structure. Using this climatology of pseudo-AE values, we can effectively convert any month of AI data to 532 nm and 1064 nm because the fixed AE is not necessarily applicable to retrieving aerosol extinction in all months. Relevant research points out that the accuracy has been improved using the corresponding AE of each month to correct the satellite data (Kovilakam et al., 2020).

Figure 10 also demonstrates the distribution characteristics of AI values at 532 nm and 1064 nm in different seasons over the TP in the daytime. In all seasons, AI is mainly distributed between -0.04 and 0.04. Still, the proportion between 0 and -0.02 is the largest. Here, we have a broad understanding of traditional AI. AI is a way to measure how backscattered ultraviolet (UV) radiation from an atmosphere containing aerosols differs from that of a pure molecular atmosphere (Guan et al., 2010). AI is especially sensitive to the presence of UV-absorbing aerosols such as smoke, mineral dust, and volcanic ash. AI, positively suggests the existence of absorbent aerosols (dust, black carbon, etc.); A small or negative AI suggests the presence of non-absorbable aerosols or clouds) (Hu et al.,2020; Guan et al., 2010; Hammer et al., 2018). AI varies with aerosol layer height, optical depth, and single scattering albedo (Torres et al., 1998;2007; Hsu et al.,2004; Jeong and Hsu, 2008). However, the significance of obtaining vertical structure AI in our research content is different from that of traditional AI representation. The AI obtained from our research work cannot effectively characterize the absorption and non-absorption of its aerosols, as the results obtained are in the non-ultraviolet band range. However, the aerosol concentration represented by the vertical structure AI is not possessed by column AOD. Compared to the aerosol column concentration AOD information, as AOD is an integral result of the entire layer height, it will to some extent lose some of the true changes in the vertical height of aerosols. The significance of our work is that the AI with higher reliability obtained here can more effectively obtain

461   aerosol concentration information at vertical height. In the four seasons, the distribution

462   of aerosols in the north is broder than that in the south; In spring, the rise height of

463   aerosol is higher and the vertical distribution range is more comprehensive. The

464   elevation in summer is lower than that in the other three seasons, but the aerosol species

465   are more abundant because there are many ranges of AE values.

466
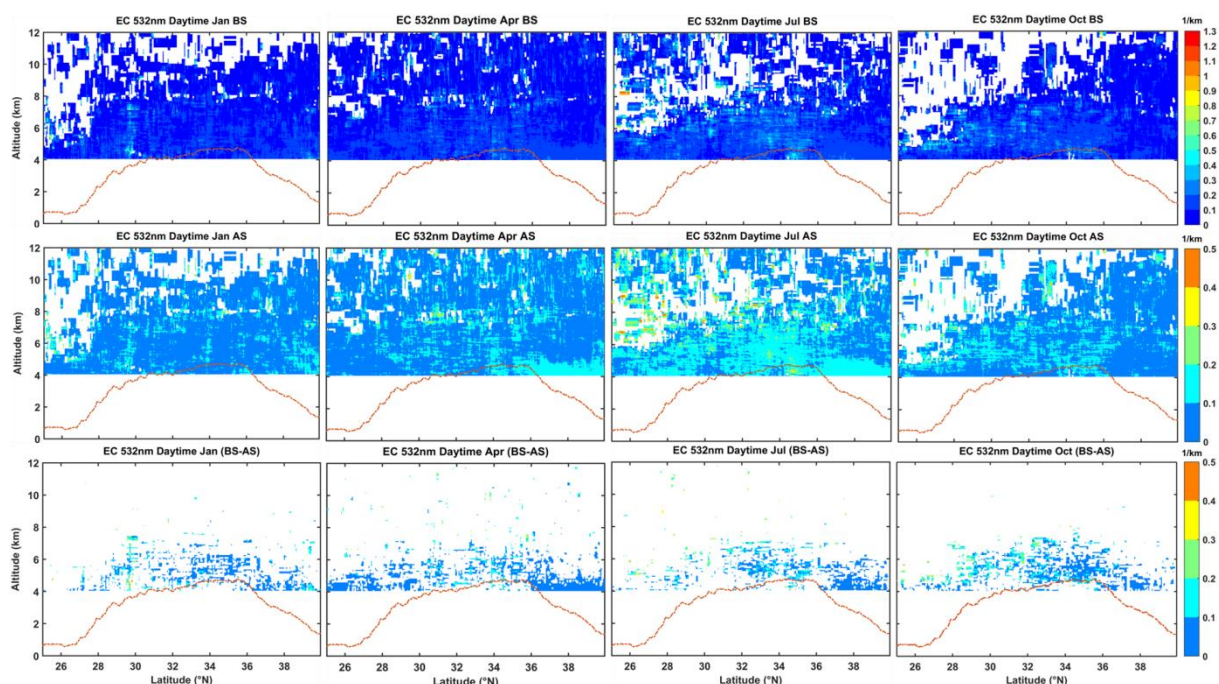
467

468   Figure 8. The monthly average comparison and difference of aerosol extinction coefficient at 532

469   nm before and after elimination of low-reliability aerosol target (LRAT) over Tibet Plateau (TP) for

470   daytime during 2007-2020. The reddish-brown dotted line denotes the surface. (BS: Before

471   Screened, first line; AS: After Screened, second line; (BS-AS) means Before Screened minus After

472   Screened, representing spatial lattice with screening and elimination, third line)

473

474
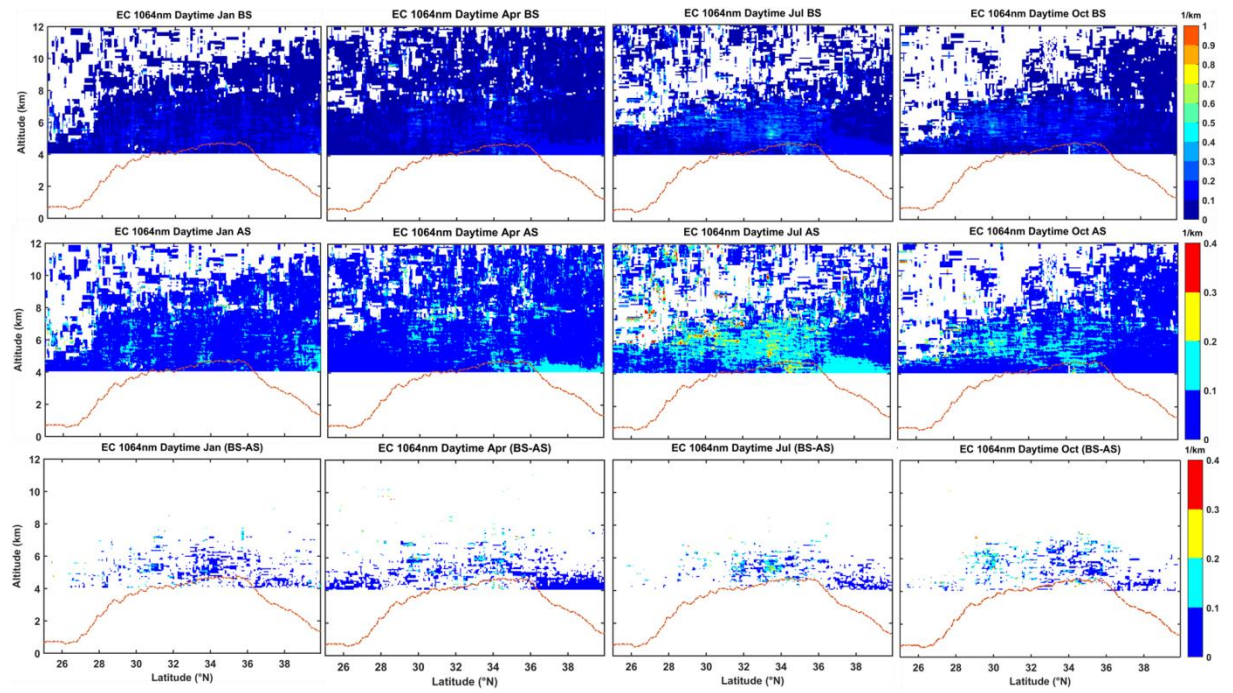
475 Figure 9. The same as in Figure 8, but for aerosol EC at 1064 nm for the daytime.

476
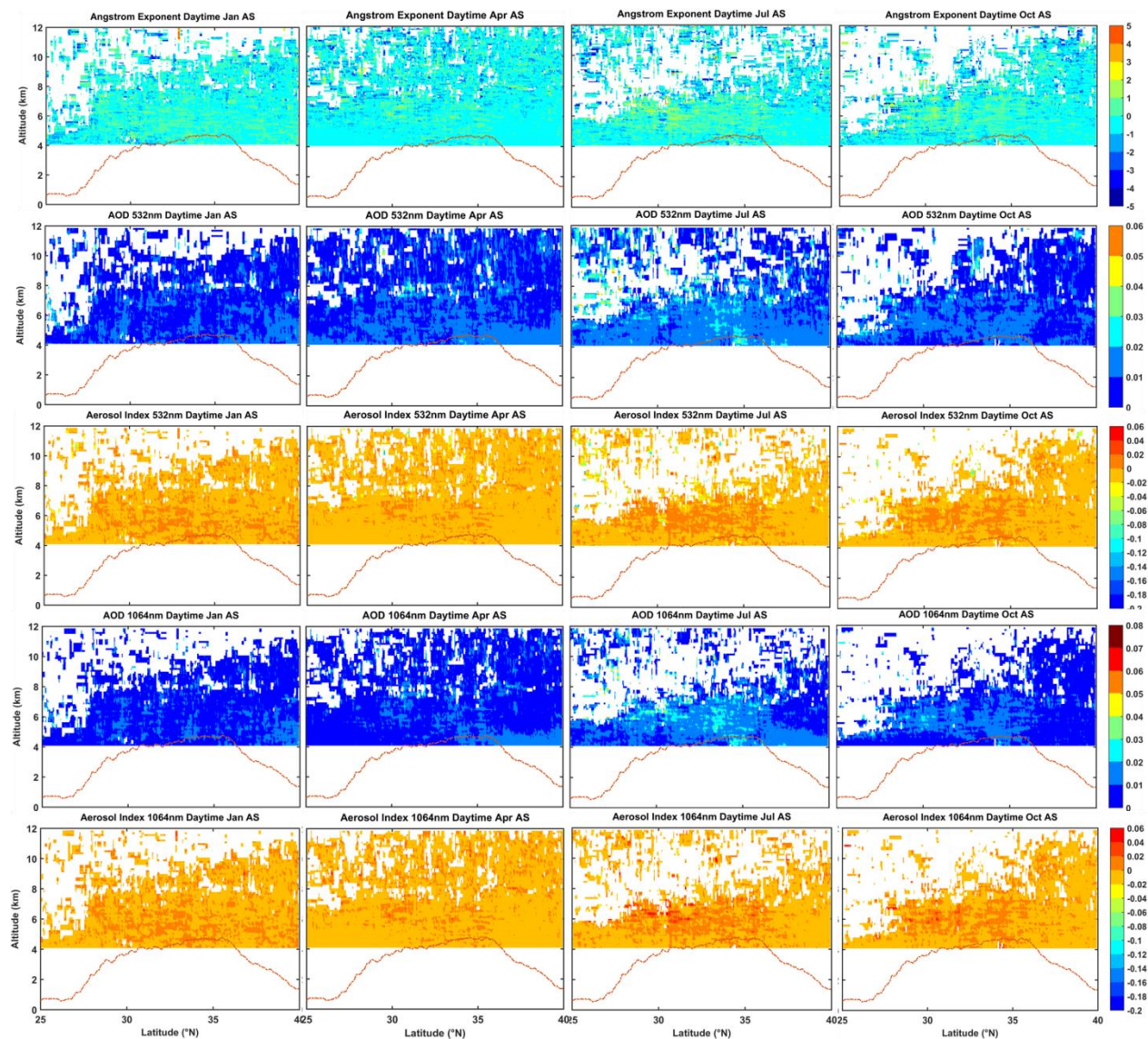
Figure 10. The monthly average construction of vertical structure of Angstrom Exponent (AE) and Aerosol Index (AI) at 532 nm and 1064 nm over Tibet Plateau (TP) for daytime during 2007-2020.

Similarly, Figure 11 includes the nighttime difference plots of aerosol EC at 532 nm between the before and after-screened for different months during 2007-2020. The difference before and after screening is immense, especially at the height of more than 5 km in the southern region of the TP in July and October. It is observed extreme outliers in the troposphere over the TP that have been recognized and eliminated. The EC detected at 1064 nm shows a similar distribution characteristic as found at 532 nm, and also includes the different attributes before and after the screened and elimination of LRAT (see Figure 12). In all seasons, AI is mainly distributed between -0.02 and 0.02. Still, the proportion between 0 and -0.02 is the largest in April and July between 4 and

8km. Meanwhile, AI above 8 km is mainly concentrated at 0-0.02, indicating modal characteristics of vertical structure distribution of aerosol concentration and diversity of aerosol types. It is worth noting that there is a large amount of aerosol over the TP in January (winter), related to anthropogenic emissions of pollutants in winter and fossil fuel combustion (such as black carbon and smoke). It is found that the pattern of AI is more or less consistent with objective facts and phenomena.

Interestingly, compared with the daytime, the aerosol detected by CALIOP at night can rise to a higher height and has a broader distribution range. It can be seen that because the signal-to-noise ratio at night is higher than that in the daytime. The CALIOP can detect smaller particles, which is also why the quality and effectiveness of CALIOP night detection data are better than that in the day. After a series of correction algorithms and calculating relevant parameters, we constructed the tropospheric AI climatology dataset over the TP for 2007-2020.
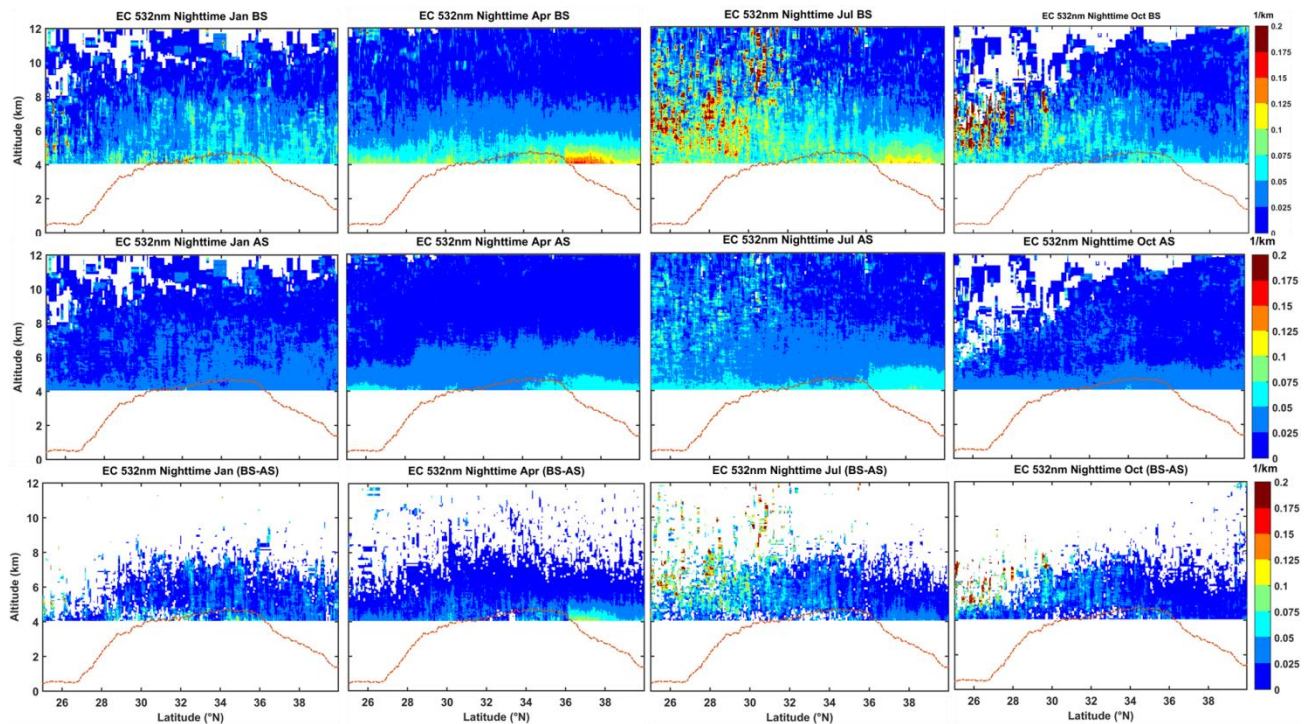
Figure 11. The same as in Figure 8, but for nighttime at 532 nm.
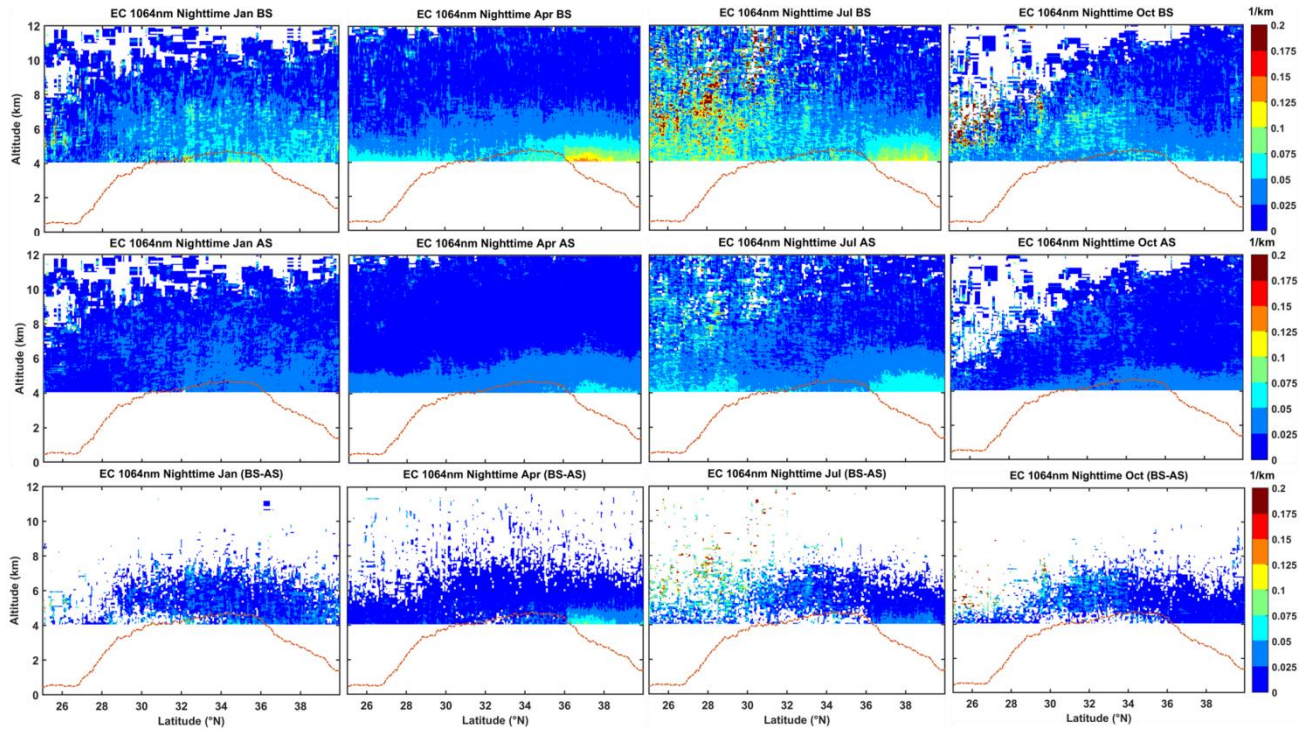
505

506 Figure 12. The same as in Figure 11, but for nighttime at 1064 nm.

507

508

509

510
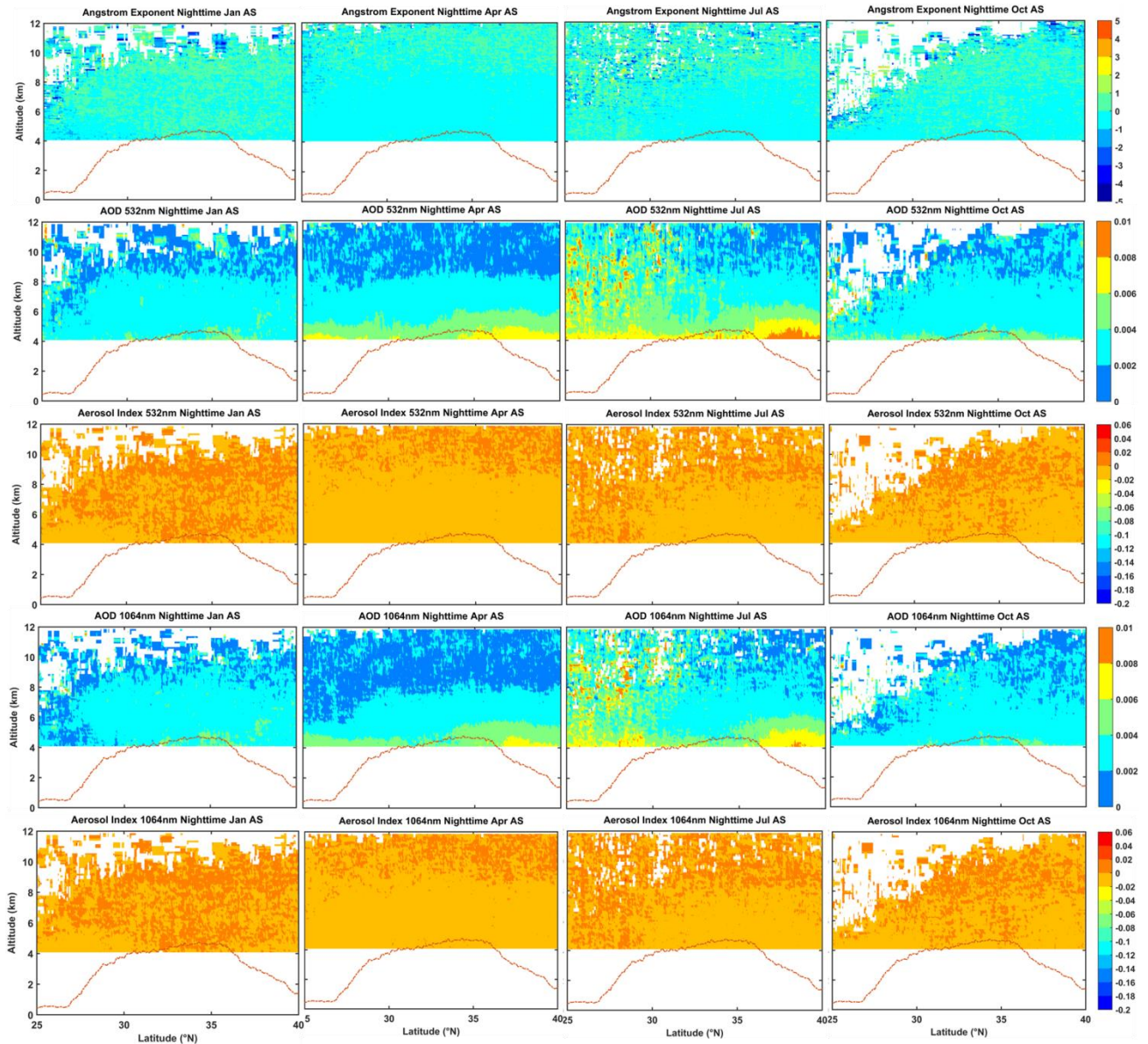
511

512 Figure 13. The same as in Figure 10, but for nighttime.

3.3 Validation of the aerosol index (AI) dataset

3.3.1 Comparisons with satellite Aqua-MODIS AI products

515   The multiyear monthly average spatial distributions of the AE and AOD from

516 MODIS have been shown in Figure 14, and AI was also calculated (Figure 14). The

517 distribution of AE values over the TP in all seasons shows a decreasing trend from

518 southeast to northwest, indicating that the particles in the upper air of the southeast

519 region are dominated by small particles. In contrast, the particles in the upper air of the

520 northwest region are dominated by large particles, especially in April of spring, which

521 is related to the uplift and transmission of dust aerosol from the Taklimakan Desert to

the northern part of the TP in spring. Also, we can see that the AE value of Taklimakan Desert in the north of the TP in April and July in spring and summer is smaller (as the source of the sand area, mainly dust aerosol), which is smaller than in January and October in autumn and winter. AOD and AE showed opposite seasonal variation distribution patterns. According to the spatial distribution pattern of AI calculated from MODIS detection results (AE and AOD), it can be seen that the AI value over the TP is mainly between 0 and 0.4.

Figure 14 also compares the normalized frequency distribution of AI over the TP exhibiting a significant difference in all seasons from MODIS and CALIOP between before and after screening. It is evident that, in general, compared with the data results without any processing, after the elimination of the low-reliability aerosol target, the average AI value of CALIOP is closer to the result of MODIS, and the normalized frequency distribution pattern is closer to the same. Interestingly, the AI mean value and normalized frequency distribution pattern of CALIOP in April (spring) after removing the LRAT are more agreement and matched with the results of MODIS; In addition, the mean AI and normalized frequency distribution pattern of CALIOP in July (summer), and October (autumn) is more consistent with the MODIS results, and both have apparent improvement. The difference between the mean AI from CALIOP in January (winter) and the result of MODIS is relatively more extensive, but the normalized frequency distribution pattern is more consistent. This may be related to the type and chemical composition of aerosol particles that rise over the TP in different seasons and the atmospheric climate conditions unique to the topography of the TP. In brief, the accuracy of aerosol parameters AI calculated after obtaining aerosol EC with higher reliability has been dramatically improved (more or less), so even though not completely accurate, this strategy is expected to reduce the inaccuracy of the computed AI at least.

Meanwhile, it is proved that using extreme outliers as a limit to get more reliable aerosol detection information is effective and reliable. It is important to note that the 550 nm wavelength range of MODIS belongs to the visible light range, and the data products provided at the satellite transit time are the daytime detection results.

Therefore, here we compare and verify the daytime detection results of CALIOP (532 nm) with MODIS results, which are consistent in time, close in detection wavelength, comparable, and representative. In addition, the quality of CALIOP daytime detection data is inferior to that at night, and the reliability and accuracy of the optimized data are more effectively verified by comparison with the results of MODIS. Passive techniques (i.e., MODIS) have the advantage of providing a 2-D distribution of AI over a wide swath, during active strategies (i.e., CALIOP) with the vertical structure of AI. They are complementary and have their advantages.
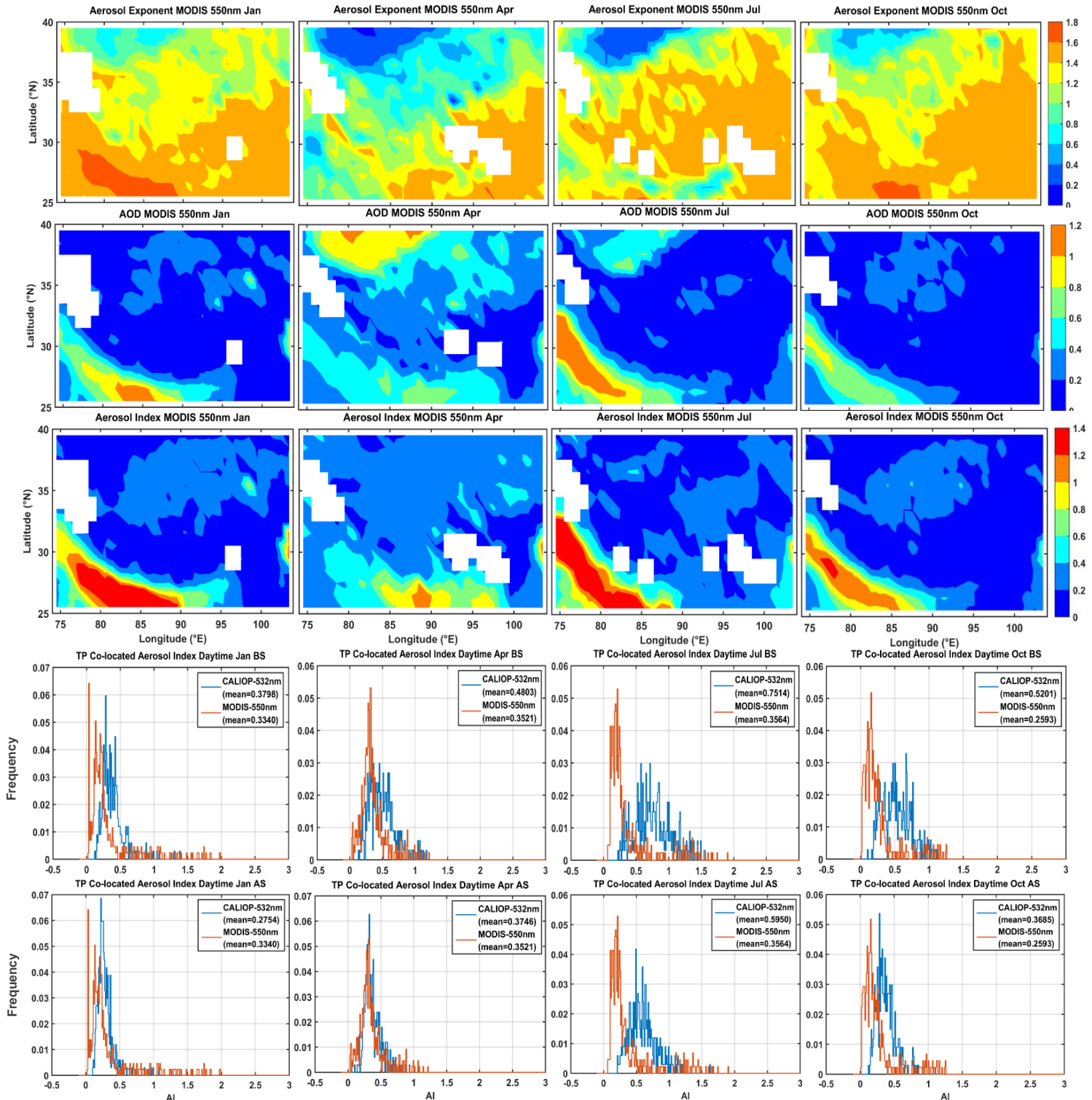
579   Figure 14. Frequency test of AI calculated by MODIS-based aerosol AE and AOD over the Qinghai

580   Tibet Plateau and AI calculated by CALIPSO-based aerosol AE and AOD with high reliability for

581   daytime (BS: Before Screened, the fourth line; AS: After Screened, the fifth line).

582   *3.3.2 Performance evaluation based on in-situ Lidar observations*

583   To further verify the performance of the AI product derived from CALIOP over

584 the TP, we chose the ground-based LIDAR observation results in the centre of the

585 Taklimakan Desert in the north of the TP to evaluate the effectiveness and accuracy of

586 the AI vertical structure of CALIOP.

587 To match the transit time of ground-based LIDAR observation and satellite

588 CALIOP observation, we extracted the EC (532 nm and 1064 nm) of ground-based

589 LIDAR during the daytime and nighttime to match the CALIOP adjacent observation

590 period, as shown in Figure 15 (observation case in TD on July 11, 2021, daytime: 03:00-

591 05:00, night: 14:00-16:00, China Beijing time, UTC+8). Considering the daytime

592 detection results of CALIOP for comparison and verification with MODIS in the above,

593 to further strengthen the inspection of CALIOP optimization results, we still choose the

594 daytime results of ground-based LIDAR detection for comparison and verification.

595 From Figure 15, it can also be seen that there are clouds or other LRAT in the daytime

596 high altitude in the ground-based LIDAR detection signal. This will be more beneficial

597 for us to check the validity and reliability of the results of the elimination of LRAT and

598 the calculated AI value.

599 Similarly, for ground-based LIDAR detection, we first reverse EC and use the IQR

600 method (see sec.2.2) to obtain extreme outliers and identify and eliminate the LRAT

601 (Figure 15). We can see that the LRAT (such as clouds and surface clutter etc.) are

602 effectively eliminated after the data optimization of 532 nm and 1064 nm detection

603 results EC. It is once again proved that it is effective and reliable to use extreme outliers

604 as a limit to obtain more reliable aerosol detection information.

605

606

607

608
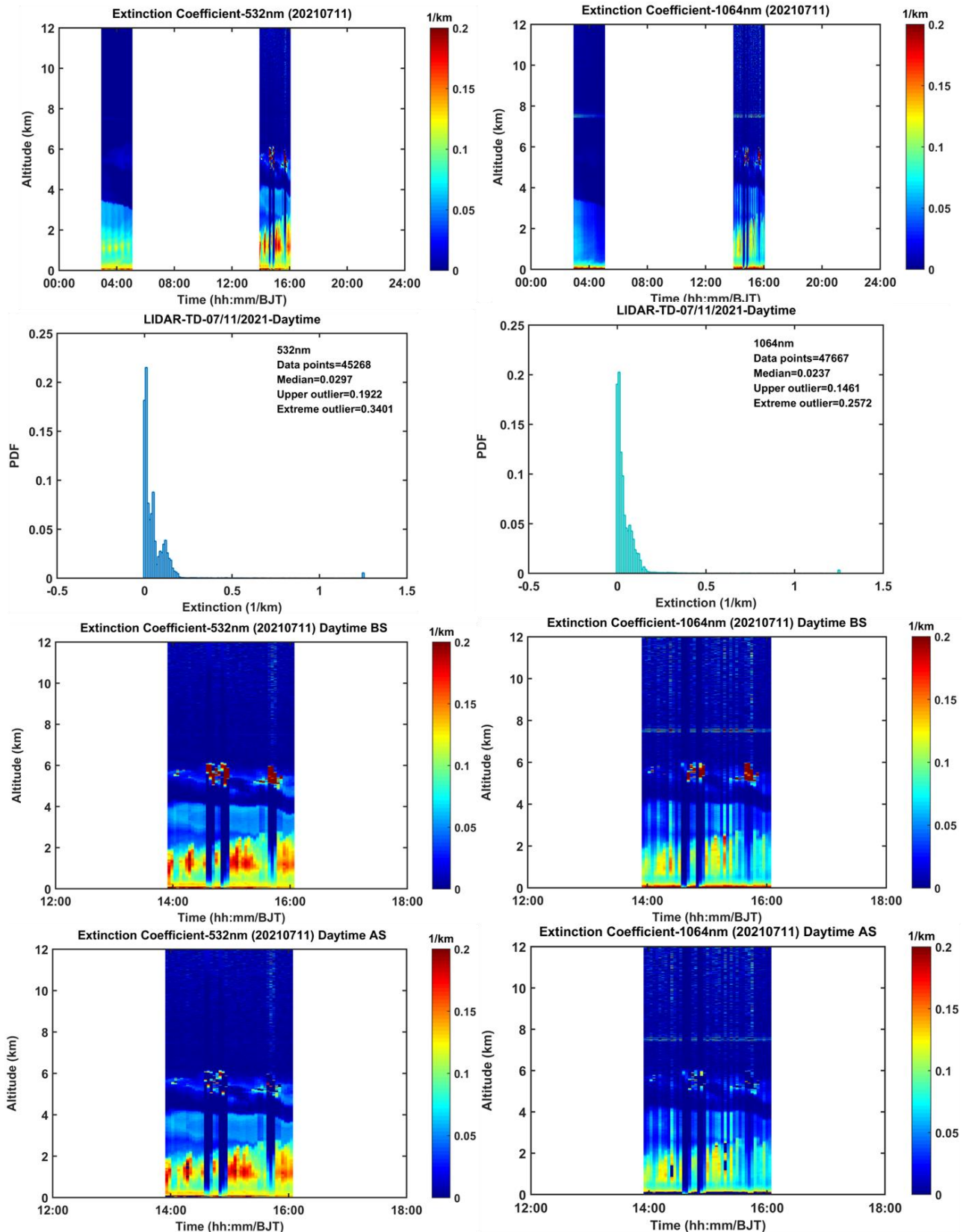
Figure 15. Elimination of low-reliability aerosol target signals detected by ground-based LIDAR in the hinterland of Taklimakan Desert.

It needs to be pointed out that the case of ground-based LIDAR detection on July

11, 2021, is quite typical, but there is a significant deviation in satellite transit, and this process cannot be well captured. To maximize and better match this process, we take the ground-based LIDAR observation in the hinterland of the Taklimakan Desert as the centre (38.967 ° N, 83.65 ° E, 1099.3m), select 38.5-39.5 ° N and 83-84 ° E range, extract the ECs observed by CALIOP transit in this range during the daytime from 2007 to July 2020, and eliminate the LRAT. After averaging the optimized data, further, calculate the AE value (as shown in Figure 16). Figure 16 depicts the detection results of ground-based LIDAR and CALIOP optimal crossing points and the comparison of calculated AI values. The AE values detected by ground-based LIDAR and CALIOP are mainly distributed between - 1 and 1, and the proportion between - 1 and 0 is the largest. The aerosol can be raised to the height of 6 km, and the higher concentration of aerosol is mainly concentrated below 2 km from the AOD vertical layer, showing a decreasing trend with the increase of height; AI values are primarily distributed between -0.02 and 0.02, and the average value and standard deviation trend of AI change with height are also basically consistent. Generally, all those facts demonstrate the agreement of the AI dataset with the CALIOP and ground-based LIDAR. Besides, all the evidence shows that after removing the LRAT, the optimized data can obtain aerosol characteristics with higher reliability.

Based on the monthly climatology AI product, we explored the average vertical structure characteristics of AI over TP during 2007-2020 (as shown in Figure 17). AI values in the daytime and at night over the TP mainly fluctuate around 0, and the standard deviation increases with the increase in altitude. The trend of AI changes with altitude is relatively consistent, and the standard deviation below 6 km is slight, indicating that the dispersion of aerosol particles is small. However, the fluctuation in the daytime is greater than that at night (the data quality at night is better than that in the daytime). In general, the detection results of 532 nm and 1064 nm can achieve complementary observation.

In general, the quality and robustness of the aerosol parameter product have improved for EC and AI with some issues that persist in the data set which we mention below:

As we do not have ground-based LIDAR detection data on the TP, we have selected ground-based LIDAR data from the centre of the Taklamakan Desert for verification and evaluation. The objectives of the verification and evaluation include the removal of low-reliability aerosol targets and the validation of the effectiveness and rationality of the constructed aerosol AI parameter results. Due to the limited detection data of ground-based LIDAR, we chose a typical aerosol process detected by ground-based LIDAR (July 11, 2021), but it did not match well with the transit time and scanning area of the CALIPSO satellite, resulting in significant errors. Therefore, we choose to compare and verify the results of the average values of July in all years within the central area of the transit Taklamakan Desert detected by CALIPSO (see the green box on the left in Figure 2). Minimize spatial errors caused by significant differences in spatial positions. This kind of error is inevitable in our data processing process and will affect the consistency of detection results to some extent.

Besides, although the monthly AI correction significantly improves the comparison between CALIPSO and MODIS, we note somewhat a larger deviation may occur in winter, and the effect after correction in summer is the best and significant, which may be related to the increased probability of mistaking clouds as aerosol particles due to more convective activities in summer. This helps us to refine our research on summer aerosols over the TP.
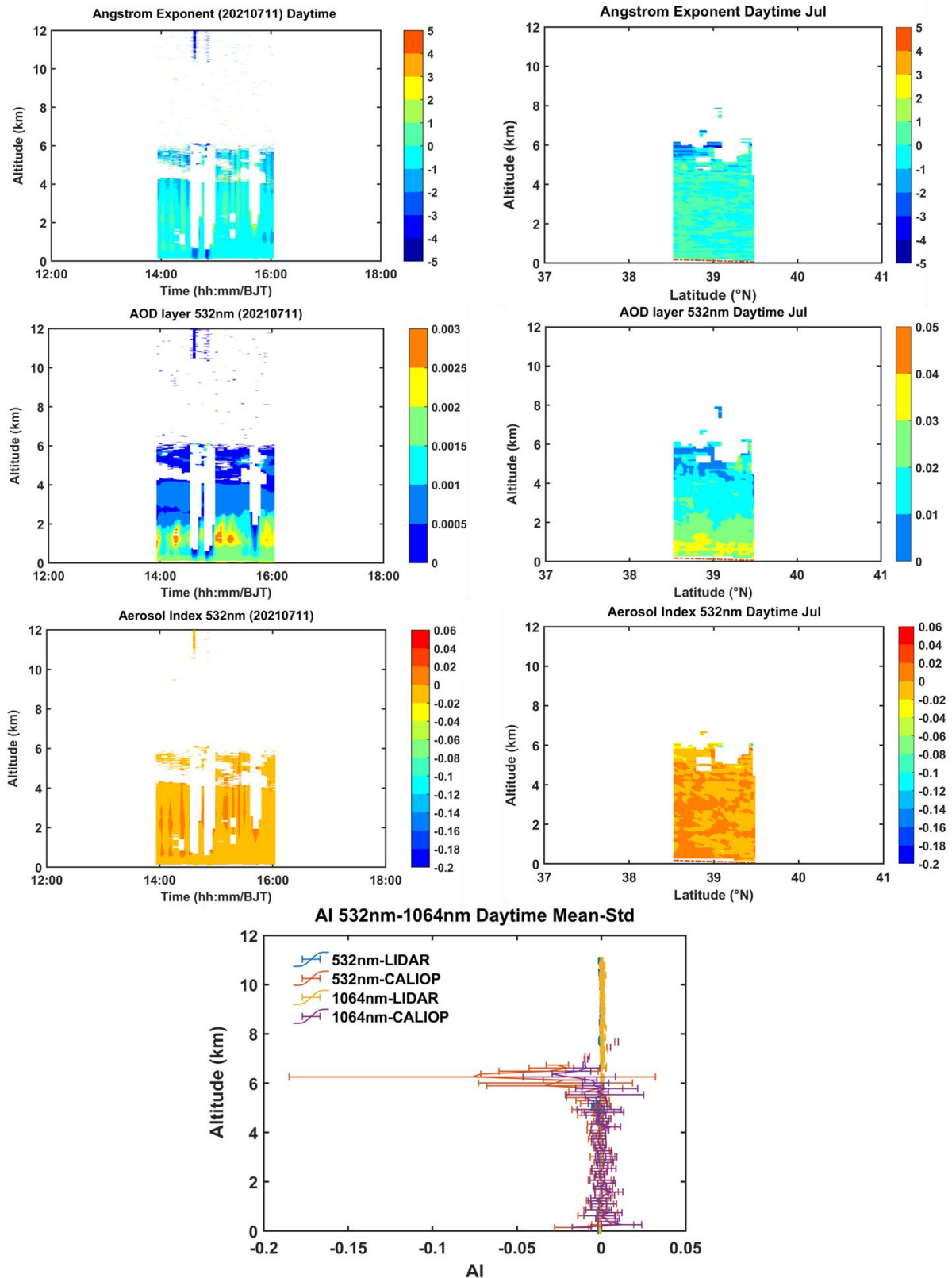
Figure 16. Comparative verification of AI of CALIPSO and ground-based LIDAR remote sensing over the Taklimakan Desert region.
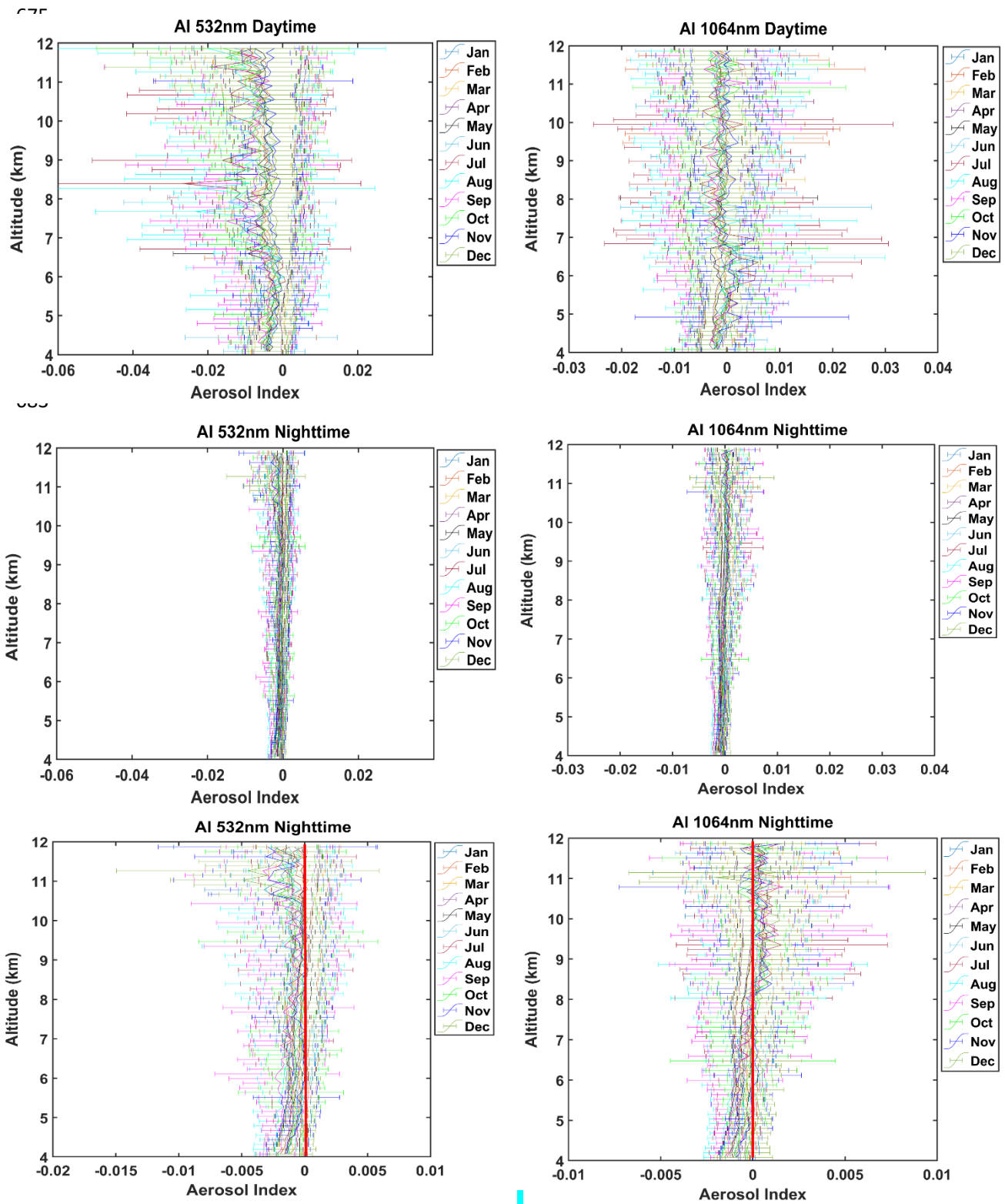
Figure 17. Monthly mean changes of vertical structure characteristics of AI (mean & standard

deviation) over TP during 2007-2020.

4 Data availability

Data described in this work are available at

https://data.tpdc.ac.cn/en/disallow/03fa38bc-25bd-46c5-b8ce-11b457f7d7fd

DOI:10.11888/Atmos.tpdc.300614. (Honglin Pan et al., 2023)

5 Summary and outlook

This present study is the first to report long-term, advanced-performance, high-resolution, continuous and high-quality, monthly climatology aerosol AI vertical structure from the CALIOP observation over the TP used to better understand aerosol radiation forcing under the background of accelerated climate change. Using the relationship developed when EC measurements are available, we screened the entire EC record. We assembled a climatology of high-altitude aerosol characteristics for daytime and nighttime from 2007 to 2020. In addition to providing a monthly climatology AI data set for MODIS and ground-based LIDAR validation, our data set also reveals the patterns and numbers of high-altitude vertical structure characteristics of the aerosol troposphere over the TP.

To produce accurate and higher reliability of AI values, we applied several correction procedures and rigorously checked for data quality constraints during the long observation period spanning almost 14 years (2007-2020). Nevertheless, some uncertainties remain mainly due to technical constraints, as well as limited documentation of the measurements. Even though not completely accurate, this strategy is expected to at least reduce the inaccuracy of the computed characteristic value of aerosol optical parameters. Following this initial work, we obtained vertical AI value with higher reliability. This provides information about the vertical structures of aerosol that could be used in climate models. The collection of more reliable and robust research data sets of aerosol characteristics in these extreme environments is the key basis for promoting comprehensive research on the energy balance of ground-atmosphere radiation over the Tibetan Plateau and even the global region. We expect that this data set will help some current and future research to simulate the climate change of the monthly climatology. It will also help to update future data sets and study the interaction

of aerosol-cloud-precipitation, thus providing sufficient observation facts and basis.

Finally, it should be pointed out that the AI obtained in the ultraviolet channel can currently characterize both absorption and non-absorption aerosols. The AI obtained from our research work cannot effectively characterize the absorption and non-absorption of its aerosols, as the results we obtained are in the non-ultraviolet band range, which is also an area that we need to further explore in the future. However, the aerosol concentration represented by the vertical structure AI we obtained is not possessed by column AOD. The significance of our work is that the AI with higher reliability obtained here can more effectively obtain aerosol concentration information and also presents a diversity of aerosol types at the vertical height over TP. This is the main highlight of our research work. The reason why we use AI to test the results of MODIS and ground LIDAR is to verify the effectiveness and reliability of AI. Fortunately, the test results are very consistent and reasonable. Therefore, the AI of physical meaning here can effectively characterize aerosol concentration information at vertical heights.

Author contributions. HP led the reprocessing of the CALIOP, LIDAR, and MODIS measurements, data analysis and the preparation of the figures, with JH and JL both contributing to the design of the paper and progression of figures and text of the article. ZH, MW and TZ made the original LIDAR measurements. ZH, AM and WH provided the dataset and advice on the re-processing of the LIDAR and CALIOP. KRK and FY contributed to either advising/co-ordinating the data recovery. All co-authors performed writing sections of the paper, and/or reviewing drafts of the paper.

Competing interests. The authors declare that they have no conflict of interest.

Acknowledgements.
We are grateful to the CALIPSO (https://eosweb.larc.nasa.gov/), MODIS (https://ladsweb.modaps.eosdis.nasa.gov/) instrument scientific teams at NASA for the provision of satellite data, and "Belt and Road" Lidar Network from Lanzhou University, China (http://ciwes.lzu.edu.cn/), which are available online and formed the central

database in the present work.

Financial support.

This work was financially Sponsored by Scientific and Technological Innovation Team (Tianshan Innovation Team) Project of Xinjiang (Grant No. 2022TSYCTD0007), the Second Tibetan Plateau Scientific Expedition and Research Program (STEP)(Grant No. 2019QZKK0602), the Natural Science Foundation of Xinjiang Uygur Autonomous Region (Grant No. 2022D01B74), National Natural Science Foundation of China (Grant No. 42005074), Scientific Research and Operation Cost Project of Urumqi Institute of Desert Meteorological, China Meteorological Administration (Grant No. IDM2020003).

References

Bucci, S., Cagnazzo, C., Cairo, F., Liberto, L.D., Fierli, F.: Aerosol variability and atmospheric transport in the Himalayan region from CALIOP 2007–2010 observations, Atmospheric Chemistry and Physics, 14(9): 4369-4381, 2014.

Boos, W., Kuang, Z.: Dominant control of the South Asian monsoon by orographic insulation versus plateau heating, Nature, 436, 218-222, 2010.

Buchard, V., Da Silva, A. M., Colarco, P. R., Darmenov, A., Randles, C. A., Govindaraju, R., Torres, O., Campbell, J., Spurr, R.: Using the OMI aerosol index and absorption aerosol optical depth to evaluate the NASA MERRA Aerosol Reanalysis, Atmospheric Chemistry and Physics, 15(10), 5743-5760, 2015.

Chen, X., Zuo, H., Zhang, Z., Cao, X., Duan, J., Zhu, C., Zhang, Z., Wang, J.: Full-coverage 250 m monthly aerosol optical depth dataset (2000–2019) amended with environmental covariates by an ensemble machine learning model over arid and semi-arid areas, NW China, Earth System Science Data, 14(12), 5233-5252, 2022.

Chen, S., Huang, J., Zhao, C., Qian, Y., Leung, L. R., Yang, B.: Modeling the transport and radiative forcing of Taklimakan dust over the Tibetan Plateau: A case study in the summer of 2006, Journal of Geophysical Research: Atmospheres, 118(2), 797-812,2013.

Chen, S., Zhang, R., Mao, R., Zhang, Y., Chen, Y., Ji, Z., Gong, Y., Guan, Y.: Sources, characteristics and climate impact of light-absorbing aerosols over the Tibetan Plateau, Earth-Science Reviews, 232, 104111, 2022.

Carrió, G. G., van Den Heever, S. C., Cotton, W. R.: Impacts of nucleating aerosol on anvil-cirrus clouds: A modeling study, Atmospheric research, 84(2), 111-131, 2007.

Guan, H., Esswein, R., Lopez, J., Bergstrom, R., Warnock, A., Follette-Cook, M., Iraci, L. T.: A multi-decadal history of biomass burning plume heights identified using aerosol index measurements, Atmospheric Chemistry and Physics, 10(14), 6461-6469, 2010.

Guan, H., Chatfield, R. B., Freitas, S. R., Bergstrom, R. W., Longo, K. M.: Modeling the effect of plume-rise on the transport of carbon monoxide over Africa with NCAR CAM, Atmos. Chem. Phys., 8, 6801–6812, doi:10.5194/acp-8-6801-2008, 2008.

Goldberg, D. L., Gupta, P., Wang, K., Jena, C., Zhang, Y., Lu, Z., Streets, D. G.: Using gap-filled MAIAC AOD and WRF-Chem to estimate daily PM2:5 concentrations at 1 km resolution in the Eastern United States, Atmos. Environ., 199, 443–452, https://doi.org/10.1016/j.atmosenv.2018.11.049, 2019.

Giles, D. M., Sinyuk, A., Sorokin, M. G., Schafer, J. S., Smirnov, A., Slutsker, I., Eck, T. F., Holben, B. N., Lewis, J. R., Campbell, J. R., Welton, E. J., Korkin, S. V., and Lyapustin, A. I.: Advancements in the Aerosol Robotic Network (AERONET) Version 3 database – automated near-real-time quality control algorithm with improved cloud screening for Sun photometer aerosol optical depth (AOD) measurements, Atmos. Meas. Tech., 12, 169–209, https://doi.org/10.5194/amt-12-169-2019, 2019.

Guan, H., Esswein, R., Lopez, J., Bergstrom, R., Warnock, A., Follette-Cook, M., Fromm, M., Iraci, L. T.: A multi-decadal history of biomass burning plume heights identified using aerosol index measurements, Atmospheric Chemistry and Physics, 10(14), 6461-6469, 2010.

Hsu, N. C., Si-Chee, T., King, M. D., Herman, J. R.: Aerosol properties over bright-reflecting source regions, IEEE Trans. Geosci. Rem. Sens., 42, 557–569, 2004.

Hammer, M. S., Martin, R. V., Li, C., Torres, O., Manning, M., Boys, B. L.: Insight into global trends in aerosol composition from 2005 to 2015 inferred from the OMI Ultraviolet Aerosol Index, Atmospheric Chemistry and Physics, 18(11), 8097-8112, 2018.

Hu, Q., Wang, H., Goloub, P., Li, Z., Veselovskii, I., Podvin, T.,Li, K., Korenskiy, M.: The characterization of Taklamakan dust properties using a multiwavelength Raman polarization lidar in Kashi, China, Atmospheric Chemistry and Physics, 20(22), 13817-13834, 2020.

Hu, Y.,S.Rodier,K.Xu,W.Sun,J.Huang,B.Lin,P.Zhai,and D.Josset.: Occurrence,liquid water content, and fraction of supercooled water clouds from combined CALIOP/IIR/MODIS measurements, J.Geophys.Res., 115, D00H34, doi:10.1029/2009JD012384, 2010.

Huang, L., Jiang, J. H., Tackett, J. L., Su, H., Fu, R.: Seasonal and diurnal variations of aerosol extinction profile and type distribution from CALIPSO 5-year observations, Journal of Geophysical Research: Atmospheres, 118(10), 4572-4596, 2013.

Huang, J., Minnis, P., Chen, B., Huang, Z., Liu, Z., Zhao, Q., Yi, Y., Ayers, J. K.: Long-range transport and vertical structure of Asian dust from CALIPSO and surface measurements during PACDEX, Journal of Geophysical Research: Atmospheres, 113(D23), 2008.

Immerzeel, W., Van Beek, L., Bierkens, M.: Climate change will affect the Asian water towers, Science, 328 (5984), 1382-1385, 2010.

IPCC: Climate Change 2013: The Physical Science Basis. Contribution of Working Group I to the Fifth Assessment Report of the Intergovernmental Panel on Climate Change, edited by: Stocker, T. F., Qin, D., Plattner, G.-K., Tignor, M., Allen, S. K., Boschung, J., Nauels, A., Xia, Y., Bex, V., and Midgley, P. M., Cambridge University Press, Cambridge, United Kingdom and New York, NY, USA, 1535 pp., 2013.

IPCC, 2021: Climate Change 2021: The Physical Science Basis. Contribution of Working Group I to the Sixth Assessment Report of the Intergovernmental Panel

on Climate Change, edited by: Masson-Delmotte, V., P. Zhai, A. Pirani, S.L. Connors, C. Péan, S. Berger, N. Caud, Y. Chen, L. Goldfarb, M.I. Gomis, M. Huang, K. Leitzell, E. Lonnoy, J.B.R. Matthews, T.K. Maycock, T. Waterfield, O. Yelekçi, R. Yu, and B. Zhou (eds.)]. Cambridge University Press, Cambridge, United Kingdom and New York, NY, USA, In press, doi:10.1017/9781009157896.

Iglewicz, B. and Hoaglin, D.: How to Detect and Handle Outliers, ASQC basic references in quality control, ASQC Quality Press, Milwaukee, 1993.

Kovilakam, M., Thomason, L. W., Ernest, N., Rieger, L., Bourassa, A., Millán, L.: The global space-based stratospheric aerosol climatology (version 2.0): 1979–2018, Earth System Science Data, 12(4), 2607-2634, 2020.

Kahn, R. A., Gaitley, B. J., Garay, M. J., Diner, D. J., Eck, T. F., Smirnov, A., Holben, B. N.: Multiangle Imaging SpectroRadiometer global aerosol product assessment by comparison with the Aerosol Robotic Network, J. Geophys. Res.-Atmos., 115, D23209, doi:10.1029/2010jd014601, 2010.

Kojima, T., Buseck, P. R., Wilson, J. C., Reeves, J. M., Mahoney, M. J.: Aerosol particles from tropical convective systems: Cloud tops and cirrus anvils, Journal of Geophysical Research: Atmospheres, 109(D12), 2004.

Kim, M.H., Omar, A.H., Tackett, J.L., Vaughan, M.A., Winker, D.M., Trepte, C.R., Hu, Y.,Liu, Z., Poole, L.R., Pitts, M.C., Kar, J., Magill, B.E.: The CALIPSO Version 4 Automated Aerosol Classification and Lidar Ratio Selection Algorithm, Atmospheric Measurement Techniques, 11(11):6107-6135,2018.

Liu, Y., Huang, J., Wang, T., Li, J., Yan, H., He, Y.: Aerosol-cloud interactions over the Tibetan Plateau: An overview, Earth-Science Reviews, 104216, 2022.

Liu, Y., Li, Y., Huang, J., Zhu, Q., Wang, S.: Attribution of the Tibetan Plateau to northern drought, National Science Review, 7(3), 489-492, 2020.

Liu, Y., Hua, S., Jia, R., Huang, J.: Effect of aerosols on the ice cloud properties over the Tibetan Plateau, Journal of Geophysical Research: Atmospheres, 124(16), 9594-9608, 2019.

Luo, H., Yanai, M.: The large-scale circulation and heat sources over the Tibetan Plateau and surrounding areas during the early summer of 1979, Part II: Heat and

moisture budgets, Mon. Wea. Rev., 112, 966–989, 1984.

Liou, K.: Influence of cirrus clouds on weather and climate processes: a global perspective, Mon. Weather Rev., 114, 1167–1199,1986.

Liu, Z., Kar, J., Zeng, S., Tackett, J., Vaughan, M., Avery, M., Pelon, J., Getzewich, B., Lee, K.P., Magill, B., Omar, A., Lucker, P., Trepte,C., Winker, D.: Discriminating between clouds and aerosols in the caliop version 4.1 data products, Atmos. Meas. Tech., 12, 703–734, 2019.

Liu, D., Z. Wang, Z. Liu, D. Winker, C. Trepte.: A height resolved global view of dust aerosols from the first year CALIPSO lidar measurements, J. Geophys. Res., 113, D16214, doi:10.1029/2007JD009776, 2008.

Liu, Z., Liu, D., Huang, J., Vaughan, M., Uno, I., Sugimoto, N., Kittaka, C., Trepte, C., Wang, Z., Hostetler, C., Winker, D.: Airborne dust distributions over the Tibetan Plateau and surrounding areas derived from the first year of CALIPSO lidar observations, Atmospheric Chemistry and Physics, 8(16), 5045-5060, 2008.

Liu, P. F., C. S. Zhao, Q. Zhang, Z. Z. Deng, M. Y. Huang, X. C. Ma, X. X. Tie.: Aircraft study of aerosol vertical distributions over Beijing and their optical properties, Tellus, Ser. B, 61(5), 756–767, doi:10.1111/j.1600-0889.2009.00440.x, 2009.

Molnar,P., Boos,W., Battisti, D.: Orographic controls on climate and paleoclimate of Asia: thermal and mechanical roles for the Tibetan Plateau, Annu. Rev. Earth Pl.Sc., 38 (1), 77-102, 2010.

Matsuki, A., Iwasaka, Y., Osada, K., Matsunaga, K., Kido, M., Inomata, Y., Trochkine, D., Nishita, C., Nezuka, T., Sakai,T., Zhang,D., Kwon, S. A.: Seasonal dependence of the long‐range transport and vertical distribution of free tropospheric aerosols over east Asia: On the basis of aircraft and lidar measurements and isentropic trajectory analysis, Journal of Geophysical Research: Atmospheres, 108(D23), 2003.

Nieberding, F., Wille, C., Fratini, G., Asmussen, M. O., Wang, Y., Ma, Y., Sachs, T.: A long-term (2005–2019) eddy covariance data set of CO_2 and H_2O fluxes from the Tibetan alpine steppe, Earth System Science Data, 12(4), 2705-2724, 2020.

Nakajima, T., Higurashi, A., Kawamoto, K., Penner, J. E.: A possible correlation

between satellite‐derived cloud and aerosol microphysical parameters, Geophysical Research Letters, 28 (7), 1171-1174, https://doi.org/10.1029/2000GL012186, 2001.

Pan, H., Huo, W., Wang, M., Zhang, J., Meng, L., Kumar, K. R., Devi, N. L.: Insight into the climatology of different sand-dust aerosol types over the Taklimakan Desert based on the observations from radiosonde and A-train satellites, Atmospheric Environment, 238, 117705, 2020.

Qiu, J.: China: The third pole, Nature, 454, 393-396, https://doi.org/10.1038/454393a, 2008.

Rossow, W., Schiffer, R.: Advances in understanding clouds from ISCCP, Bull. Am. Meteorol. Soc., 80, 2261‐2287, 1999.

Rieger, L. A., Bourassa, A. E., Degenstein, D. A.: Merging the OSIRIS and SAGE II stratospheric aerosol records, J. Geophys. Res. Atmos., 120, 8890–8904, https://doi.org/10.1002/2015JD023133, 2015.

Rieger, L. A., Zawada, D. J., Bourassa, A. E., Degenstein, D. A.: A Multiwavelength Retrieval Approach for Improved OSIRIS Aerosol Extinction Retrievals, J. Geophys. Res.-Atmos., 124, 7286–7307, https://doi.org/10.1029/2018JD029897, 2019.

Seifert, P., Ansmann, A., Müller, D., Wandinger, U., Althausen, D., Heymsfield, A. J., Massie, S.T., Schmitt, C.: Cirrus optical properties observed with lidar, radiosonde, and satellite over the tropical Indian Ocean during the aerosol-polluted northeast and clean maritime southwest monsoon, Journal of Geophysical Research: Atmospheres, 112(D17), 2007.

Sasano, Y.: Tropospheric aerosol extinction coefficient profiles derived from scanning lidar measurements over Tsukuba, Japan from 1990 to 1993, Appl. Opt., 35(24), 4941–4952, 1996.

Thomason, L. W. and Vernier, J.-P.: Improved SAGE II cloud/aerosol categorization and observations of the Asian tropopause aerosol layer: 1989–2005, Atmos. Chem. Phys., 13, 4605–4616, https://doi.org/10.5194/acp-13-4605-2013, 2013.

Twomey, S.A.: The influence of pollution on the shortwave albedo of clouds, J. Atmos.

945 Sci., 34 (7), 1149 – 1154,1977.

946 Torres, O., Bhartia, P. K., Herman, J. R., Ahmad, Z., and Gleason, J.: Derivation of

947  aerosol properties from satellite measurements of backscattered ultraviolet

948  radiation: Theoretical basis, J. Geophys. Res., 103, 17099–17110,

949  doi:10.1029/98JD00900, 1998.

950 Torres, O., Tanskanen, A., Veihelmann, B., Ahn, C., Braak, R., Bhartia, P. K., Veefkind,

951  P., Levelt, P.: Aerosols and surface UV products from Ozone Monitoring

952  Instrument observations: An overview, J. Geophys. Res., 112, D24S47,

953  doi:10.1029/2007JD008809, 2007.

954 Vernier, J. P., Fairlie, T. D., Natarajan, M., Wienhold, F. G., Bian, J., Martinsson, B. G.,

955  Crumeyrolle, S., Thomason, L.W., Bedka, K. M.: Increase in upper tropospheric

956  and lower stratospheric aerosol levels and its potential connection with Asian

957  pollution, Journal of Geophysical Research: Atmospheres, 120(4), 1608-1619,

958  2015.

959 Wan, B., Gao, Z., Chen, F., Lu, C.: Impact of Tibetan Plateau surface heating on

960  persistent extreme precipitation events in Southeastern China, Mon. Weather Rev.,

961  145 (9), 3485–3505, 2017.

962 Winker, D. M., Vaughan, M. A., Omar, A., Hu, Y., Powell, K. A., Liu, Z., Hunt, W. H.,

963  and Young, S. A.: Overview of the CALIPSO mission and CALIOP data

964  processing algorithms, J. Atm. Ocean. Techn., 26, 2310–2323, 2009.

965 Winker, D.M., Hunt, W.H., McGill, M.J.: Initial performance assessment of CALIOP,

966  Geophys. Res. Lett., 34, L19803, https://doi.org/10.1029/2007GL030135, 2007.

967 Wu, G., Zhang, Y.: Tibetan Plateau forcing and the timing of the monsoon onset over

968  South Asia and the South China Sea, Mon. Wea. Rev., 126, 913-927,1998.

969 Wu, G., Liu, Y., Zhang, Q., Duan, A., Wang, T., Wan, R., Liu, X., Li, W., Wang, Z.,

970  Liang, X.: The influence of mechanical and thermal forcing by the Tibetan Plateau

971  on Asian climate, J. Hydro. Meteor. Spec. Sect., 8 (4), 770-789, 2007.

972 Wu, G., Liu, Y., Dong, B., Liang, X., Duan, A., Bao, Q., Yu, J.: Revisiting Asian

973  monsoon formation and change associated with Tibetan Plateau forcing: I.

974  Formation, Climate dynamics, 39, 1169-1181, 2012.

Wu, G., Duan, A., Liu, Y., Mao, J., Ren, R., Bao, Q., He, B., Liu, B., Hu, W.: Tibetan Plateau climate dynamics: recent research progress and outlook, Natl. Sci. Rev., 2 (1), 100-116, 2015.

Wei, X., Bai, K., Chang, N.-B., Gao, W.: Multi-source hierarchical data fusion for high-resolution AOD mapping in a forest fire event, International Journal of Applied Earth Observation and Geoinformation, 102, 102366, https://doi.org/10.1016/j.jag.2021.102366, 2021.

Xu, X., Lu, C., Shi, X., Gao, S.: World water tower: an atmospheric perspective, Geophys. Res. Lett., 35 (20), 2008.

Xu, C., Ma, Y. M., You, C., Zhu, Z. K.: The regional distribution characteristics of aerosol optical depth over the Tibetan Plateau, Atmospheric Chemistry and Physics, 15(20), 12065-12078, 2015.

Yanai, M., Li, C., Song, Z.: Seasonal heating of the Tibetan Plateau and its effects on the evolution of the Asian summer monsoon, J. Meteor. Soc. Japan 70, 319-351,1992.

Zhang, S., Huang, Z., Li, M., Shen, X., Wang, Y., Dong, Q., Bi J., Zhang J., Li W., Li Z., Song, X.: Vertical structure of dust aerosols observed by a ground-based raman lidar with polarization capabilities in the center of the Taklimakan desert, Remote Sensing, 14(10), 2461, 2022.

Zhang, S., Huang, Z., Alam, K., Li, M., Dong, Q., Wang, Y., Shen, X., Bi, J., Zhang, J., Li, W., Li, Z., Wang, W., Cui, Z., Song, X.: Derived Profiles of CCN and INP Number Concentrations in the Taklimakan Desert via Combined Polarization Lidar, Sun-Photometer, and Radiosonde Observations, Remote Sensing, 1–20. https://doi.org/10.3390/rs15051216, 2023.

Zhou, J., G. Yu, C. Jin, F. Qi, D. Liu, H. Hu, Z. Gong, G. Shi, T. Nakajima, T. Takamura.: Lidar observations of Asian dust over Hefei, China in Spring 2000, J. Geophys. Res., 107(D15), 4252, doi:10.1029/,2002.2001JD000802, 2002.